Environmental data collection and analyses to support conservation planning in the Israeli EEZ

October 2022

Shabtay Ateret[1], Goren Liron[2,3], Slavenko Alex[4], Idan Tal[3,5], Neuman Adi [6], Bialik Or [6,7], Makovsky Yizhaq [6,8]

[1] *Society for the Protection of Nature in Israel*

[2] *Steinhardt Museum of Natural History*

[3] *School of Zoology, George S. Wise Faculty of Life Sciences, Tel Aviv University*

[4] *Fenner School of Environment & Society, College of Science, The Australian National University*

[5] Department of Biomolecular Science, The Weizmann Institute of Science

[6] *The Strauss Department of Marine Geosciences, Leon H. Charney School of Marine Sciences, University of Haifa*

[7] *Marine Geology and Seafloor Surveying, Department of Geosciences, University of Malta*

[8] *The Hatter Department of Marine Technologies, Leon H. Charney School of Marine Sciences, University of Haifa*

The Blue Half Project of the Society for the Protection of Nature in Israel is an NGO promoting a comprehensive environmental reform to protect the marine ecosystems in the Israeli Mediterranean Sea. The reform focuses on establishment of marine reserves, sustainable fisheries management, endangered species protection, conservation-oriented marine spatial planning, and public participation in marine conservation. The Israeli EEZ MPAs Masterplan initiative is a conservation planning process aiming to balance between development and conservation in the Israeli EEZ, and to reach the spatial target of 30% marine protected areas by 2030.

Summary

The Israeli EEZ in the Mediterranean Sea is subjected to several current and future anthropogenic pressures. The area currently lacks significant measures that can balance conservation and economic development, especially marine spatial planning and marine protected areas. The "Israeli EEZ MPAs masterplan" project is a systematic conservation planning initiative aiming to outline a proposal for well connected, representative and efficient network of marine reserves.

The first step of this process is collecting environmental data that can supply spatial data on conservation features, such as representative, unique habitats and key species as a basis for the plan.

A hierarchical classification system for ecological units was selected for the bioregionalization process (identifying distinct biogeographic regions). At the broadest level we related to biogeographic concepts, and at finest level we used cluster analysis, diversity and dissimilarity measures to characterize biological assemblages. Then, we identified Vulnerable Marine Ecosystem (VME) indicators in the area according to available data (9 VME indicator species and 2 indicator habitats). These indicators were used in distribution modelling to calculate the probability of unique habitats presence.

We Identified 18 representative benthic ecological units with changing degrees of certainty regarding their faunal composition. The distribution model yielded strong indication for VME presence in over 3% of the EEZ, and additional Medium-strong indication for VME presence in over 14% of the EEZ.

The results of this work are to be revised by the project's scientific advisors and then by a scientific committee. Besides evaluating the quality of this work and its products, the revision process will be used as experts' consultation for deciding on conservation targets and other parameters to be included in the next stage of the project – Spatial conservation prioritization using Marxan.

Glossary

ANOSIM: Analysis of Similarity

AOO: Area of Occupancy

AUC: Area Under the ROC Curve

BRT: Boosted Regression Tree

CART: Classification and Regression Tree

D^2: Deviance Explained

EEZ: Exclusive Economic Zone

FORed: Functional Over-redundancy

FRed: Functional Redundancy

FVuln: Functional Vulnerability

GAM: Generalised Additive Model

GDM: Generalised Dissimilarity Model

GFCM: General Fishing Commission for the Mediterranean

GLM: Generalised Linear Model

GSI: Geological Survey of Israel

IOLR: Israel Oceanographic and Limnological Research

IUCN: International Union for Conservation of Nature

MARXAN: Marine Spatially Explicit Annealing

MaxEnt: Maximum Entropy

MPA: Marine Protected Area

PCA: Principal Components Analysis

PCoA: Principal Coordinates Analysis

RF: Random Forest

ROC: Receiver-Operating Characteristic

SDM: Species Distribution Models

SIMPER: Similarity Percentage

TSS: The Sum of Sensitivity and Specificity

VME: Vulnerable Marine Ecosystem

Table of Content

Introduction

Marine conservation planning is the process of locating areas that will be primarily managed for conservation objectives aiming to promote the persistence of biodiversity and other natural values. Habitats and natural regions are used in conservation planning as planning units. This allows for MPA network to reflect the key principles of MPAs design: Comprehensiveness, adequacy and representativeness (Grorud-Colvert et al. 2021). For this purpose, the process requires spatial data of habitats and species distribution in the area of the plan. This data is then used for **bioregionalization** - a process by which the physical and biological variability in the environment is analyzed, classified and mapped into spatial units, each with distinct biological, ecological and physical properties (Dunstan et al. 2020).

Although there are several approaches for marine bioregionalization and habitat classification schemes, most are using **hierarchical classification systems** where regions are identified on a range of **hierarchically nested scales** (Howell et al. 2010). Using a hierarchical scheme has several advantages such as providing context for spatial information and common reference for discussion and decision making (Harris 2020).

Marine habitats hierarchical classification schemes are widely described in the scientific literature, and many were successfully applied around the globe. Most schemes are "rule-based", meaning that different levels in the hierarchy are defined on the basis of a theory that explains the difference between levels (Poiani et al. 2000). For example, range of physical parameters that apply over broad area (e.g., Roff et al. 2003), physiographic provinces and geomorphology of the sea floor (e.g., Greene et al. 1999), or range of bioregions (e.g., Madden and Grossman 2004). A scheme developed in Australia by Last et al. (2010) was especially designed for the selection of a **national representative system of MPAs**. This scheme integrates biological and physical criteria, with emphasis on different criteria at different levels in the hierarchy (see Figure 1.).

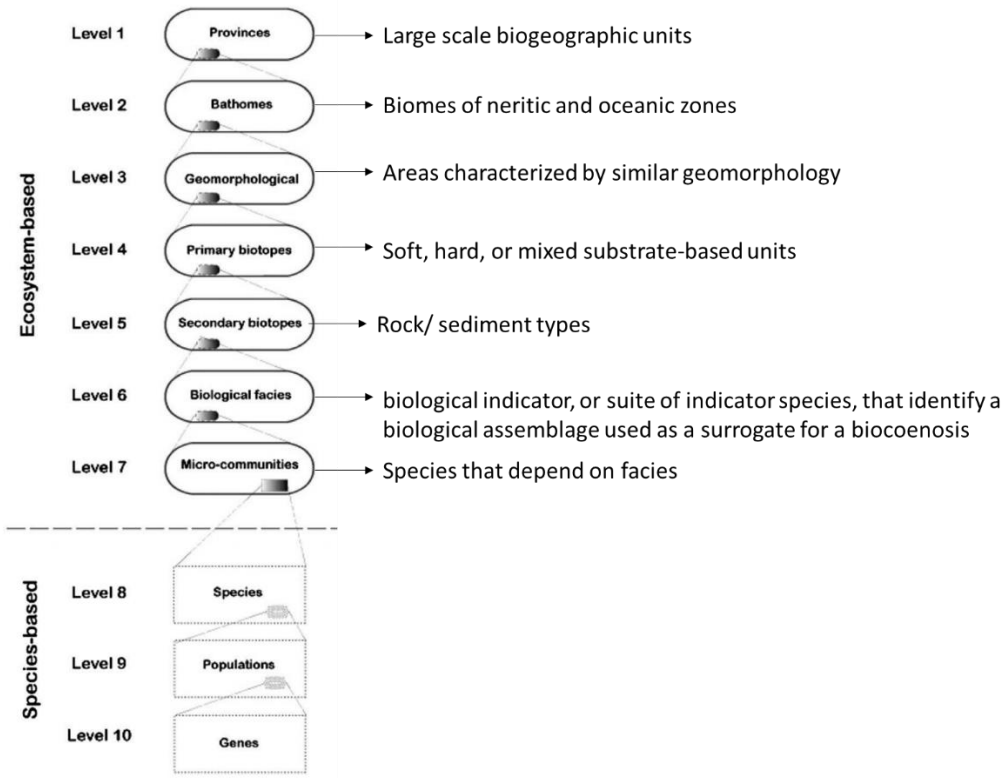

Figure 1. The conceptual hierarchical framework used for classifying seabed biodiversity as applied to marine resource planning and management in Australia. It shows the 10 nested levels existing within an ocean realm. Adopted from Last et al. (2010).

Hierarchical classification systems have the intrinsic predictive power of describing the **relationships between physical habitats and their associated biological communities**. Thus, a hierarchical classification system must be able to be modified when missing components are identified (Roff and Taylor 2000). This is especially important and useful for bioreginalization of deep-sea areas where biogeography concepts are less developed and significant data gaps exist for faunal distribution, biology, and ecosystem functionality (Howell 2010, IUCN 2019). In addition, although knowledge of biological facies distribution in deep-sea bioregion is important for setting conservation priorities, some facies are spatially restricted or rare and may be misrepresented in a broad-scale bioreginalization. These are often most vulnerable to anthropogenic impacts and may need to be given a high conservation priority. For example, oases of vulnerable and unique biological assemblages at the muddy plains of the deep sea such as chemosynthetic ecosystems around cold seeps, coral gardens and sponge grounds. An adequate representation of these key conservation features in the planning process, can be achieved by using species distribution models to predict presence of these habitats in vast underexplored areas of the deep sea (Rengstorf et al. 2012, Cordes et al. 2016).

The **Israeli EEZ in the Mediterranean Sea** is subjected to several anthropogenic pressures and is currently lacking significant measures that can balance conservation and economic development. Currently, there are neither MPAs declared, nor a comprehensive planning that considers conservation priorities, and environmental and planning legislation is partial. Future pressures are expected to rise and climate change impacts to increase.

Benthic and pelagic habitats in the EEZ were previously described, to some degree, in the strategic environmental assessment conducted by the Israeli Ministry of Energy's project between 2014 and 2016[1]. The survey intended to form a knowledge base and act as a decision making tool for the Petroleum Commissioner in granting petroleum exploration and production rights offshore Israel, aiming to minimize potential harm to the ecosystem while evaluating other benefits of environmental, social, and economic value. The results of the survey and further updates that were performed along the years, highlighted limited presence of highly vulnerable, yet rare, benthic habitats in the region. However, since the scope of the survey was not conservation-planning oriented, the ability of the products to fully represent habitats' variability and complexity in the Israeli EEZ is limited.

The "Israeli EEZ MPAs masterplan" project is a systematic conservation planning initiative led by the SPNI in collaboration with the ministry of environment, academia and IOLR. The need in conservation planning, planning principles, objectives and project's structure are all detailed in the **background document of the project[2]**. The first step of this process is collecting and analyzing previously collected environmental data as the basis for the MPA planning.

This report presents the environmental data collection and analyses for the Israeli EEZ MPAs masterplan project. The work was carried out between July 2021 and July 2022. The main products of this work include the following **spatial data layers**:

[1] https://www.energy-sea.gov.il/English-Site/Pages/Data%20and%20Maps/Strategic-Environmental-Assessment-(SEA).aspx , the survey conducted by Geo-prospect and IOLR

[2] The background document written in Hebrew in 2022. See Appendix 3.

1. **Representative benthic ecological units**
2. **Unique benthic habitats**

For each of these products, the report includes a detailed methodology section on data collection and analyses performed, results section, and discussion that aims to highlight key issues for consultation and decision-making.

The products of this work should be adjusted following peer-review and scientific consultation with experts prior to their use in a spatial prioritization for conservation in the next stage of the project. Moreover, the products should be subjected to updates following new finding and data collection that are expected in the area in the near future.

Methods

Study area

The area of the plan is the Israeli EEZ (hereafter = EEZ). It spans 22,000 km^2, about 100-180 km from the coast and beyond the territorial waters[3] (see Figure 2). The area borders the Lebanese EEZ[4] in the north, The Egyptian EEZ in the south, and the Cyprus EEZ in the west. Depth ranges from about -200 m in the east and about 2500 m in the west.

Figure 2. Area of the plan – The Israeli exclusive economic zone in the Mediterranean Sea

Data collection

Biotic data

Biological data was obtained from a literature review on the species and habitats present in the Israeli EEZ (Table 1 and Annex 5). The final dataset included spatial information on about 800 taxa, belonging to phyla ranging from Porifera through Annelida and Mollusca to Fish, Reptiles and mammals. Additional data exist from the area but could not be used as it is inaccessible to us due to security regulations.

Thereafter, we collected taxonomical information to each taxon using the WORMS[5] database, making sure that all species names and taxonomic affiliations are correct and up-to-date to avoid overlaps. We also used Fishbase[6], Sealifebase[7], scientific papers, and WORMS to collect

[3] 32.9707681°E 32.8974153°N, 33.8898422°E 33.6568865°N, 34.8825870°E 33.1820763°N, 34.1057453°E 32.6768777°N, 34.1057453°E 32.6768777°N

[4] Negotiations for determining the maritime border between Israel and Lebanon are ongoing

[5] https://www.marinespecies.org/

[6] https://www.fishbase.se/search.php

[7] https://www.sealifebase.ca/

zoogeographic (habitat, collection coordinates, depth range, local or invasive), and ecological data (feeding guilds, size group, sensitivity according to the IUCN), to determine each taxon's ecological attributes.

Table 1. Data sources, sampling methods and number of observations of biological data collected

Data source	Data type	Sampling methods	Number of observations
Peer-reviewed papers	Deep-sea expeditions (such as the Meteor) and biological studies on deep-sea organisms from the Levant	Grab and core sampling of sediment, trawling and ROV video surveys	2171
Scientific reports conducted by Oil and Gas companies (submitted to the Israeli Ministry of Energy)	Surveys conducted around sites of gas drilling wells, before and after drilling commenced, in accordance with the license provided by Israeli government	Box-corer and visual data collected by ROV	
Scientific reports conducted by IOLR	Surveys conducted for monitoring purposes from 1993 until 2022, scientific research and the strategic environmental assessment (see footnote 1)	Trawling and box-corer	3050
Data submitted to online databases[8]	Deep-sea expeditions and scientific research data uploaded to un open access database	Box-corer and visual data	87
Unpublished data from ROV footages and samples	Nautilus 2010 and 2011, SEMSEEPS 2016 and 2017 CSMS-IOLR joint ROV cruise onboard RV Bat-Galim, in the framework of MERCI[9]. Analyzed by several researchers in the frame of	Visual data collected by ROV	999

[8] https://obis.org/
[9] https://merci.haifa.ac.il/?lang=en

	AMEL[10] (Weissman, A., Ezra, O., Goren, L., Idan, T., and Reinhard, W.)		

All data were converted to GIS feature classes, where data with a single coordinate was stored as a point feature, and data with two coordinates (i.e., trawls) was stored as a polyline feature. Since the spatial accuracy in most cases was not recorded, we removed any data for which sampling method was unknown or assumed to be with a very low spatial accuracy.

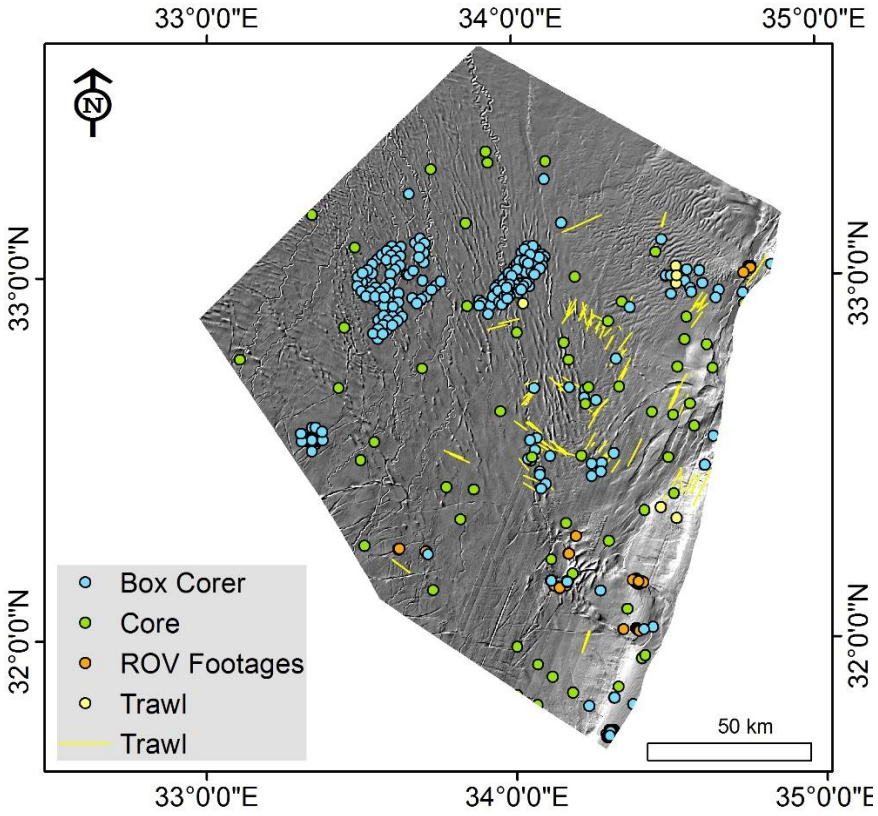

Figure 3. Sampling points in the EEZ. Major data sources include IOLR surveys (i.e. IOLR 2016), gas companies surveys and academic researches.

Abiotic data

To estimate typical fields of physical and chemical parameters on different levels we used observations extracted from Cast DB of IOLR[11] for the period between 1990 and 2020 to avoid bias related to the Eastern Mediterranean Transient (Incarbona et al. 2016). For surface layer (3 m level) and 100 m level all parameters calculated separately for summer season (July-September) and winter season (January-March). For levels below 100 m all observation was used without seasonality

[10] AMEL - Applied Marine Exploration
[11] https://isramar.ocean.org.il/isramar_data/CastMap.aspx

The observations from the DB are arranged in vertical casts. The interpolation procedure was carried out with vertical interpolation to constant depth levels and a bottom level, followed by horizontal interpolation to a rectangular grid. For the calculation of values at the bottom layer, we used gridded bathymetry[12] () and collected the deepest values of observation casts in which the bottom of the cast is at most 50 m above the gridded bathymetry. For constant depth levels, observations on each relevant cast were linearly interpolated. The horizontally scattered observations on each level were interpolated using the Kriging tool in the commercial software "SURFER" (Golden software company). Kriging assigns weights to the surrounding measured values in deriving a prediction for an unmeasured location. Within Surfer, Kriging can be either an exact or a smoothing interpolator depending on the user-specified parameters. It incorporates anisotropy and underlying spatial trends in an efficient and natural manner. The grid geometry (544 rows x 580 columns, Xmin = 32.789583°, Xmax = 35.202083°, Dx = 0.004167°, Ymin = 31.489583°, Ymax = 33.752083°, Dy = 0.004167°) includes the Israeli EEZ. The Kriging tool was set to replace multiple observations within 2E-07° of each other by their median value. For each grid point, the Kriging tool only considers the influence from observations that are within 1.28° of that point. The grids after Kriging were smoothed by low-pass numerical filter averaging 9-nodes (3x3). See maps in Annex 4).

Table 2. Abiotic parameters used in the analyses, number of sampling stations and sampling periods. For benthic ecological units analyses, only data collected within the 50 m above seafloor was used.

Variable	Numbers of stations	From date	To date
Concentration of carbon (organic)	48	3/10/2013	3/15/2013
Concentration of carbon (total inorganic)	50	3/10/2013	3/15/2013
Concentration of nitrate+nitrite	227	8/12/1990	3/16/2020
Dissolved oxygen	611	8/12/1990	3/16/2020
Concentration of phosphate	240	3/10/2013	3/16/2020
Concentration of silicate	205	8/12/1990	3/16/2020
Practical salinity	669	8/12/1990	3/16/2020

[12] https://www.gebco.net/data_and_products/gridded_bathymetry_data

Temperature	666	8/12/1990	3/16/2020

Bathymetric data and attributes

The Israeli EEZ has been fully mapped with multibeam by the IOLR at a resolution of 25 m, with data quality varying between regions (Kanari et al., 2020). However, due to imposed national security limitations the data was only made available to our analysis at the publically released 100 m resolution. Bathymetric data was therefore obtained from the highest resolution alternative sources: Kanari et al. (2020) bathymetric multibeam digital elevation model (DEM, in resolution of 100 m), Gvirtzman et al., 2015 seafloor picks of 3D seismic data (normally obtained at a 12.5 m grid resolution), and local multibeam grids (provided at 50 m resolution) . All data were calibrated to Kanari et al. (2020) DEM, combined and re-grided to a uniform 25 m resolution. The bathymetric attributes where then measured from the high resolution data and mapped to the 2 km resolution of our modeling, providing the maximal or averaged values and the standard deviation or range in each 2 km grid cell. This allowed for ecological units analyses at 2 km grid to be based on high resolution attributes.

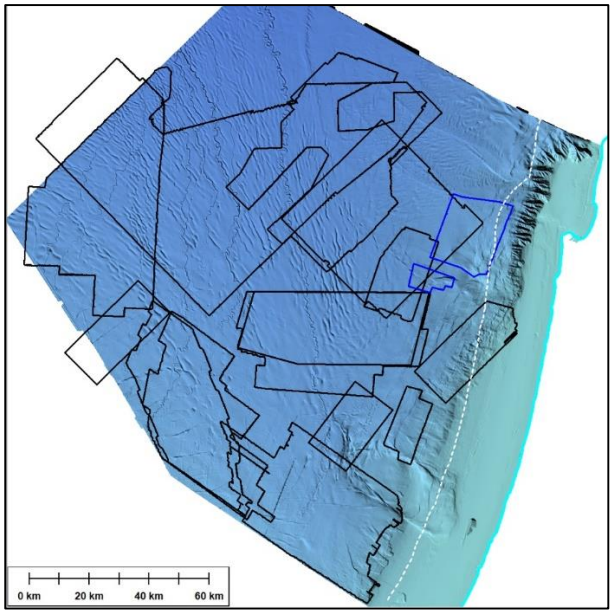

Figure 4. The bathymetric datasets combined to form the 25 m resolution DEM, which was used for extracting the bathymetric attribute maps. Blue outlines are areas where multibeam data was available at a resolution of 25-50 m. Black outlines are areas where seismic data was normally available at a resolution of 12.5 m.

Representative benthic ecological units

In the current project we adopted the Australian habitats classification system developed by Last et al. (2010), since this scheme is clearly planning oriented and presets classification levels that can be

produced using the existing data available for the Israeli EEZ. Slight adjustments to Last et al. (2010) methodology were preformed to fit the existing available data and area characteristics:

- Levels 4 and 5 were merged- Substrate diversity is low in the Israeli EEZ and does not justify two classification levels of biotopes.
- Levels 6 and 7 were merged for some of the facies and communities in areas where sampling did allow for indicator species identification or where taxonomic identification was inconsistent and could therefore bias indication.

After adjustments, the hierarchical classification system for benthic ecological units included five levels as presented in Figure 5.

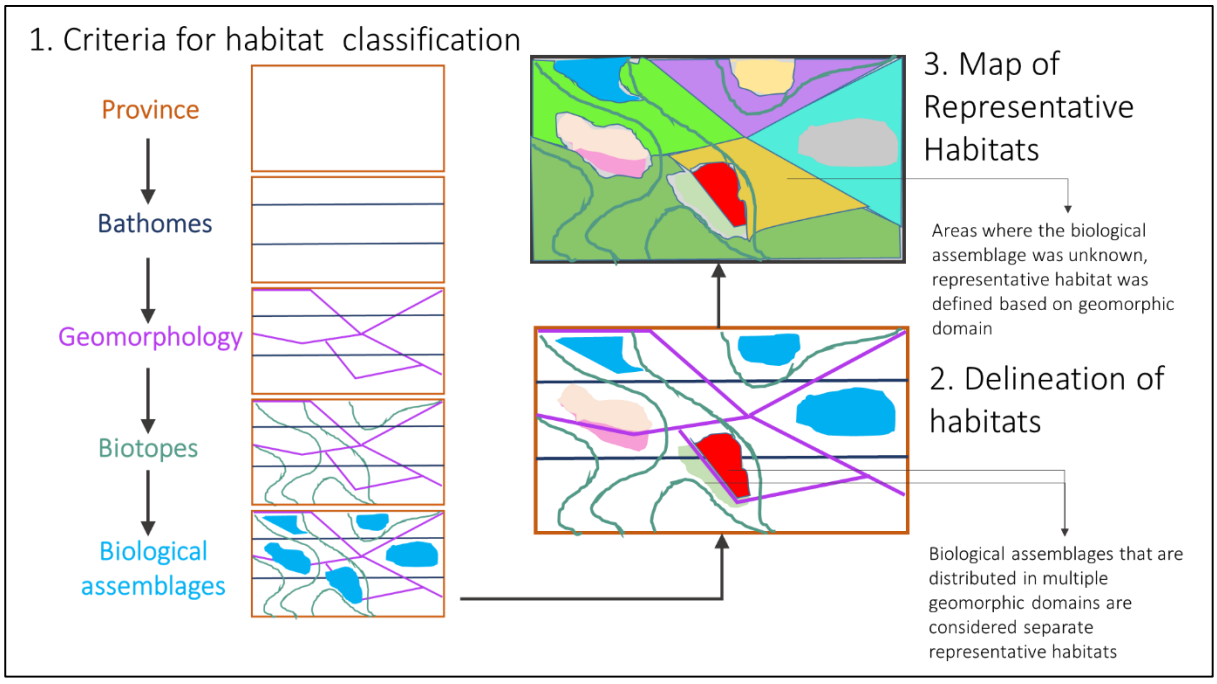

Figure 5. Hierarchical levels used in bioregionalization of the Israeli EEZ and conceptual ecological units delineation process.

Province

Characterized as Mediterranean Sea - Levantine basin, based on common biogeographic features (see Annex 1).

Bathomes

Based on commonly used classifications for the area and water masses classification suggested by IOLR (2016), three bathymetric depth ranges were defined for the EEZ: 200-600 m, 600-1000 m and below 1000 m (see Annex 1).

Geomorphology

Geomorphic domains were defined based on the features described by Gvirtzman et al. (2015) and Kanari et al. (2020) and the Hydrate stability boundary estimated to intersect the seafloor of the EEZ at the water depth of ~1200-1300 m (Figure 6 and see Annex 1).

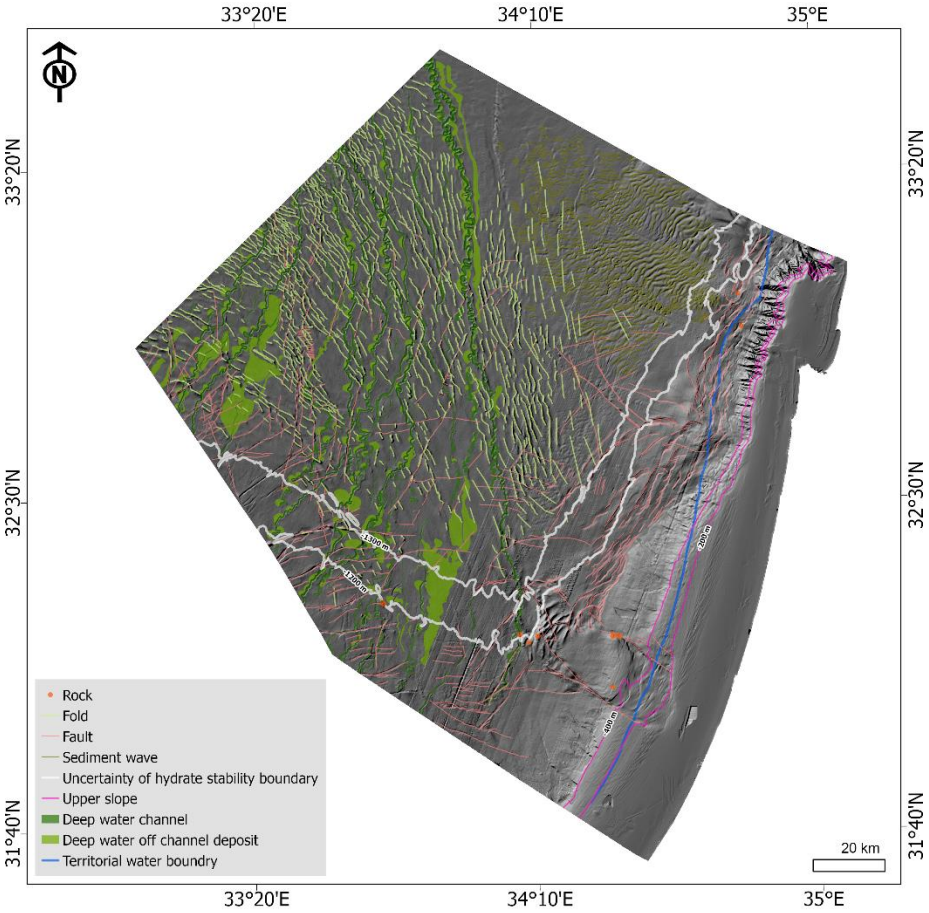

Figure 6. Geomorphic features in the EEZ adopted from Kanari et al. (2020). The features were used to define geomorphic domains. For detailed description of the features, see Annex 1.

Biotopes

Grain size distribution data was adopted from Elyashiv and Kruvi (2016). Sediment distribution was re-modelled in the EEZ using the bulk sediment d10, d50, d90, clay fraction, silt fraction, sand fraction and total organic carbon data. Initial analysis included a principal component analysis (PCA) and a correlation matrix analysis to identify codependences between the different observed sedimentary properties, and their relation with the sampled seafloor water depth. Based on clustering in the PCA space, the data were split into two subsets across the 600m bathymetric isobath. Each subset had gone through a second correlation matrix analysis with water depth included as a parameter. The correlation was tested for linear and non-linear relationships. Linear relationships with water depth were modelled using simple linear regression. Non-linear relationships with water depth were defined by seeking an optimal fit. Where no significant relations could be found with the water depth, modelling was carried out using identified dependencies on an intermediate parameter (see Table 3).

Table 3. The following relation and transformation types were used to model the parameters (for a detailed specification of the regression equations used see Annex 1):

		d10	d50	d90	%clay	%silt	%sand	%TOC
Above 600m	Modelling parameter	Water depth	Water depth	Water depth	Water depth	Water depth	Water depth	Water depth
	Relations	Linear*	Power	Power	Log-Linear	Log-Linear	Power	Log-Linear*

Below 600m	Modelling parameter	Water depth	%silt	%sand	%silt, %sand	Water depth, longitude	Water depth	Water depth
	Relations	Log-Linear	Linear	Log-Linear	Delta	Log-Linear	Exp Polynomial	Log-Linear

*only data below a water depth of 120m were used.

The resulting equations were used to populate a lat/long grid with a 0.1° resolution across the EEZ, this grid was then interpolated using triangulated irregular network (TIN).

Biological assemblages

The biological data set used for biological assemblage characterization consisted of 332 taxa obtained from 4009 observations[13]. Data were projected onto a grid consisting of 0.1*0.1 decimal degree cells – all observations within cells were combined to generate a presence/absence matrix of taxa, after dropping cells with only a single taxon. Data cleaning included exclusion of observations where: 1. the taxonomic identification only included class or higher levels, and/or 2. the sampling method was unclear, and/or 3. The spatial reference was unclear. In addition, taxa with questionable identification (e.g., taxa that are unknown to occur in the Mediterranean Sea) were excluded based on expert opinion. Furthermore, conservative approach was adopted to avoid over-counting of taxa, by merging several taxa into higher taxonomic level, to prioritize the less specific identification in cases where specific identification (e.g., to species level) was unavailable.

[13] The remaining 468 taxa for which distribution and ecological data was collected, and which were not used for biological assemblage characterization are available for use as background information for the plan and further analyses if necessary. These mostly include Chordata which are generally less useful for characterizing benthic habitats.

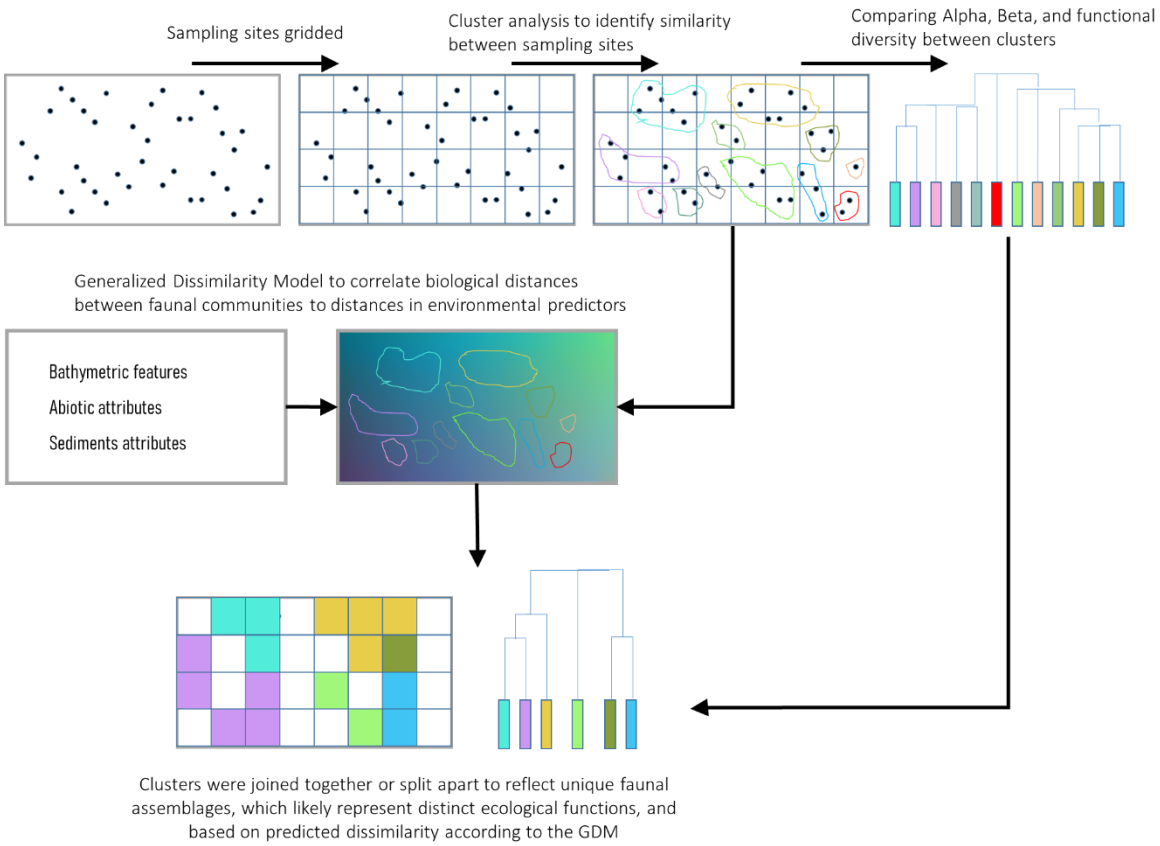

Figure 7. Conceptual process of biological assemblage characterization process

The clustering methodology followed (Castro-Insua et al. 2018). Dissimilarity between cells was calculated using the Simpson dissimilarity index (Simpson 1960) to minimize bias caused by variation in alpha diversity as a result of unequal sampling effort, methods, periods, and taxonomic analyses in the EEZ. Simpson dissimilarity was calculated by partitioning Sorensen dissimilarity into turnover and nestedness components (Baselga 2010) using the *beta.pair* function in the 'betapart' package v1.5.6 (Baselga et al. 2022), and extracting the turnover component (equal to Simpson dissimilarity).

Hierarchical clustering was performed on the dissimilarity matrix using the *hclust* function with the Ward clustering algorithm. Optimal number of clusters was selected using Analysis of Similarity (ANOSIM) tests on *k* clusters ranging from 2 to 50. The ANOSIM test statistic R was then plotted against *k*, and the optimal *k* was chosen as the minimal value for which *k*+1 did not cause a relevant increment in the ANOSIM R statistic, determined by visually assessing the plots (see results, Figure 10).

To visualize and compare patterns of diversity between cells and clusters we calculated:

- Alpha diversity for each cell and cluster with Simpson index (Simpson 1949). Then, Beta diversity was calculated between clusters using Sorensen dissimilarity, partitioned into turnover and nestedness components. High degrees of nestedness between clusters were treated as indicative of clusters belonging to the same biological assemblage.
- Functional diversity for each cluster by combining different taxa into distinct functional entities (Table 4). Functional entities were defined based on food guild and habitat type (benthic carnivore, infaunal deposit feeder, etc.). Functional richness was calculated as the number of functional entities in each cluster. Three indices of functional diversity were then calculated for each cluster (Mouillot et al. 2014):

1. Functional redundancy – the average number of taxa per functional entity.
2. Functional over-redundancy – the proportion of taxa in functional entities above the mean level of functional redundancy.
3. Functional vulnerability – the proportion of functional entities with only a single taxon.

It is important to note that these variables were not used for clustering but only for more comprehensive description and further investigation of the clusters.

Table 4. List of functional entities and the habitat types and food guilds they represent

Functional Entity	Habitat Type	Food Guild
fe_1	Infauna	Deposit Feeder
fe_2	Infauna	Filter Feeder
fe_3	Infauna	Carnivore
fe_4	Benthic	Carnivore
fe_5	Benthic	Suspension Feeder
fe_6	Benthic	Deposit Feeder
fe_7	Benthic	Omnivore
fe_8	Benthic	Filter Feeder
fe_9	Infauna	Omnivore
fe_10	Benthopelagic	Carnivore
fe_11	Infauna	Suspension Feeder
fe_12	Benthic	Herbivore
fe_13	Benthic	Chemosymbiont
fe_14	Infauna	Parasite

A Generalized Dissimilarity Model (GDM) was constructed to correlate biological distances between faunal communities to distances in environmental predictors. The abiotic features used for the GDM are detailed in Annex 1.

Uncertainty around the I-splines depicting the functional responses of compositional dissimilarity to each environmental predictor was plotted using a subsampling bootstrapping. 100 bootstraps at 70% subsampling, were run. Spatial predictions for compositional dissimilarity were then generated for each environmental predictor based on the final GDM model, and the predictions were projected onto three-dimensional ordinated space using a PCA. The PC values were then scaled to RGB color channels to generate a map where dissimilarity in colors represents predicted biological dissimilarity.

Using the final biological assemblage polygons, additional SIMPER were run to calculate the contribution of each taxon in a community matrix to dissimilarity. Pseudo-abundance was calculated for each biological assemblage as the sum of unique observations per taxon (since abundance data are needed for this analysis). Taxa that contribute at least to 70% of the difference between each pair of biological assemblages were identified as the most important to differentiation between assemblages.

For each discrete biological assemblage, descriptions of the habitat, justification for grouping, and defining features are provided (see Results section and Annex 1).

To quantify uncertainty in the definition of the biological assemblages, five different measures were calculated, all relating to uncertainty in faunal composition (rather than assemblages' spatial extent). These measure can be used to evaluate the degree of which the assemblages represent distinct compositions of taxa:

1. Proportion of each taxon's area of occupancy (AOO; calculated following International Union for Conservation of Nature (IUCN) recommendations on methodology to calculate area of occupancy, by summing the number of 2km^2 cells in which the taxon is present) represented within the biological assemblage (Bland et al. 2017). The higher this proportion, the more this taxon is unique to the assemblage, with 100% representing an endemic species. This measure was averaged across all taxa in each assemblage.
2. Proportion of endemic taxa, calculated for each biological assemblage as the number of endemic taxa divided by the total number of taxa recorded there.
3. Proportion of the assemblage's area represented in the taxon's AOO. The higher this proportion, the more common and widespread the taxon is throughout the area of the assemblage. This measure was averaged across all taxa in each assemblage.
4. Sampling density per km^2, calculated as the number of unique samples divided by the area of the assemblage.
5. Taxonomic identification, ranging from 1 (identified to phylum level) to 5 (identified to species level). This measure was averaged across all taxa in each assemblage.

These five measures were then converted to rank orders, to generate a relative certainty, with 1 being the least certain assemblage, and 5 being the most certain. The rank orders of the five measures were averaged to generate a final, relative certainty measure for each biological assemblage. Certainty scores were also calculated using a weighted and unweighted average approach to examine sensitivity to weighing.

All analyses for characterizing biological assemblages were performed in R v4.1.3 (R Core Team 2022).

In addition to the biological assemblages that were identified, we included biological assemblage of unique epibenthic habitat described by Hyams-Kaphzan et al. (2018) and Almogi-Labin and Hyams-Kaphzan (2016) and classified using Foraminiferous species. The GDM map was used to roughly mark the boundaries of this assemblage. Certainty score for this assemblage was qualitatively defined as 1.

Delineating representative ecological units

Each biological assemblage was delineated in the context of and according to the levels above it to define representative ecological unit. Where biological assemblages are unknown, ecological units were delineated based only on the above level, and especially by the geomorphic domain that are known to have relatively high predictive power of habitats distribution (see Figure 5).

Unique benthic habitats

To assess the possible extent of VMEs in the EEZ, several indicator taxa for the presence of VMEs were chosen. The taxa chosen are either habitat forming species, as well as taxa which are known to be strongly associated with VMEs. Following a thorough literature review, and considering the International Union for Conservation of Nature (IUCN) and General Fishing Commission for the Mediterranean (GFCM) guidelines, a list of approximately 110 taxa was compiled, whose presence in the surveyed area could potentially indicate the presence of a dozen types of VMEs. This list was further filtered to include only the taxa whose level of indication for VMEs was considered high or medium (~80 taxa, see Annex 1), and that had a sufficient sample size (9 taxa).

Species Distribution Models (SDM) were constructed using an ensemble approach (Araújo and New 2007), and based on the same environmental predictor layers that were used to construct the representative ecological units GDM (see above).

Table 5. List of indicator species considered in the species distribution models, the VME they inhabit, and the level of indication they provide for its presence.

Name	Group	Number of observations	VME
Antipathes dichotoma	Black corals	153	Coral gardens
Isidella elongata	Black corals	60	Coral gardens
Swiftia pallida	Black corals	189	Coral garden
Viminella flagellum	Sea pens	38	Coral gardens
Chemosytnhetic tube worms	Polychaeta	22	Cold seeps
Lamellibrachia anaximandri	Polychaeta	19	Cold seeps
Thyasira flexuosa	Bivalvia	7	Cold seeps
Funiculina quadrangularis	Sea pens	88	Sea pen fields
Rhizaxinella shikmonae	Sponges	23	Soft bottom sponge ground

For each species, 500 pseudo-absences were randomly generated across the EEZ. Environmental variables for each point, both presences and pseudo-absences, were then extracted from each predictor layer. The data were then randomly divided into a 70% training set used to build the SDMs, and a 30% test set for validation. Six different algorithms were used to construct SDMs from the training set:

1. Generalised Linear Models (GLMs) were fitted with a binomial family and logit link function, for both linear and quadratic terms of the predictor variables. Automated stepwise model selection based on AIC scores was then performed using the *step* function to remove non-informative predictor variables.

2. Generalised Additive Models (GAMs) were fitted with the *gam* function in the "gam" package v1.20.1 (Hastie 2022), using smooth splines with 4 degrees of freedom for each predictor variable.

3. Classification and regression trees (CARTs; Franklin 2010, Guisan et al. 2017) were fitted using the *rpart* function in the "rpart" package v4.1.16 (Therneau and Atkinson 2022). Internal cross-validation (xval) and minimum number of observations available to define a split (minsplit) were set at their default values of 10 and 20, respectively.

4. Random Forests (RFs; Hastie et al. 2009, Guisan et al. 2017) were fitted using the *randomForest* function in the "randomForest" package v4.7-1.1 (Liaw and Wiener 2002). The number of trees to grow (ntree) was set at 1000.

5. Boosted Regression Trees (BRTs) were fitted using the *gbm.step* function from the "dismo" package v1.3-5 (Hijmans et al. 2021), The Bernoulli (=binomial) family was used, tree.complexity was set at 2, and bag.fraction and learning.rate were set at their default values of 0.75 and 0.001, respectively.

6. Maximum Entropy (MaxEnt; Phillips et al. 2006, Elith et al. 2011) models were fitted using the *maxent* function in the "maxnet" package v0.1.4 (Phillips 2021).

Using the 30% test set, several different measures of model performance were calculated. The optimal threshold for converting continuous predictions to binary (presence/absence) was chosen by optimising the sum of sensitivity and specificity (TSS), calculated by generating a confusion matrix from the observed and predicted test data to assess the frequencies of true positive results (sensitivity) and true negative results (specificity). Additionally, the area under the curve (AUC) of the receiver-operating characteristic (ROC) was calculated, which can be interpreted as the chance of assigning a higher predicted occurrence probability to a presence compared to an absence point, with values over 0.9 interpreted as excellent predictive capability (Araújo et al. 2005). Finally, the deviance explained (D^2) by the prediction in the test set was calculated.

Using the environmental layers, spatial predictions for the probability of occurrence of each taxon were calculated with each of the six SDMs. Then, ensemble predictions were generated for each taxon using four different types of aggregation: mean probability, median probability, weighted mean probability (weighted by TSS), and committee average of binary predictions (The proportion of models predicting a presence above the optimal threshold). The best method of aggregation for each taxon was selected by maximising TSS, AUC, and D^2, in that order.

To generate predicted probabilities for the presences of the different VMEs, predicted probability maps of the best ensemble model for each taxon were clipped to only include probabilities above the optimal threshold. Then, a weighted mean of the predicted probabilities of all indicator taxa in each VME was calculated (weighted by TSS of the best ensemble models) to generate the probability of VME presence in each cell. Predicted probabilities were set at 1 in cells where indicator taxa were directly observed.

Finally, a relative certainty score for the VME prediction maps were generated by calculating the standard deviation between the six SDM predictions for each taxon, and calculating the mean SD across all indicator taxa for each VME. SD was set at 0 in cells where indicator taxa were directly observed, and was then converted to a certainty index, ranging from 0 to 1, and inversely proportional to SD - thus, in the extreme cases, cells with a certainty of 1 and predicted probability of 1 represent absolute certainty of VME presence, cells with a certainty of 1 and predicted probability of 0 represent absolute certainty of no evidence for VME presence (all models for all indicator taxa predict below the suitability threshold), and cells with a certainty of 0 indicate high uncertainty regarding the prediction for VME presence or absence (model predictions greatly differ from one another).

Gas seep pockmarks and Rocky Habitat distribution possibility

Gas seep pockmarks and rocky habitat distribution possibility was performed using ArcGIS Pro (v.2.9.3) and was created for 2X2km grid by combining three models:

1. For the areas of 'Palmahim A', 'Palmahim B' and 'Palmahim C', we generated a reduced version of the potential map as described in Makovsky et al. (2020).

2. The possibility model for the southern ‘deep-sea fan’ and ‘base of slope’, was generated based on pockmarks observations using fuzzy logic method. First, the observations were weighted according to Makovsky et al. (2020). Then for each weight class, we generated a separate raster to represent the distance from each pockmark within the same class. The generated rasters were transformed to a scale of 0-1 by using the ‘small’ non-linear function. A ‘midpoint’ of 1500 and a ‘spread’ value of 1, were used. The result rasters were then multiplied by the assigned weight, and merged by giving the maximum value in case of overlapped cell.
3. The north part of base of slope, was modeled using similar method as previous described. However, in this case the distance from a fault was also considered as a condition, since it was found to be correlated to the number of observed pockmarks. For this purpose, we used Kanari et al. (2020) faults mapping, and summed the transformed ‘distance-to-fault’ raster with the transformed ‘distance-to-pockmark’ raster using weighted sum method. Where the later condition was weighted twice higher.

Results

Representative benthic ecological units

Detailed description of the hierarchical levels used for classifying representative ecological units are available in Annex 1. The following results include the main new findings that were used for the classification.

Considering the combined impact of the geomorphological factors, and the resulting seafloor morphology, we define 10 large scale geomorphic domains as the basis for classifying the representative ecological units of the Israeli EEZ:

Upper Slope. Delineated by the 200m isobath to the east (marking the edge of the continental shelf) and the 400m isobath to the west. The 400m isobath marks the top of the head scars of large submarine landslides in the central and southern part of the slope. This area is characterized by a gentler inclination relative to the rest of the slope.

Lower Slope. Delineated by the 400m isobath to the east and the base of slope (defined by the regional structural change of the slope., which is not necessarily aligned with an isobath) to the west. This area includes the slumps and submarine landslides along the southern and central part of the slope and the canyons at the north part of it.

Base Slope. Delineated by the base of slope to the east and the 1250m isobath (top of the hydrate stability field) to the west. This area is characterized by extensive presence of small pockmarks and active gas seepage in some locals.

Palmahim C. Outlined by the head scar of the Palmahim Disturbance (PD), which forms a local depression with enhanced dips relative to its surrounding to the east, north and south. This area is characterized by stepped topography and transport of material from the surrounding highs, and possibly rocky outcrops and some small pockmarks.

Palmahim B. Defined as a union of the coral gardens areas (as defined in Makovsky et al. (2020)) and bounded to the east by the Palmahim C area and to the west by the simpler central part of PD. This area is elevated from its surrounding to the north and south, forming complex bathymetry at the drops of both sides, and is characterized by a complex and varied geomorphology. Authigenic carbonates are known in several localities across this area, notably to the north and south of it, colonized by unique cold water coral communities.

Palmahim A. Delineated by the Levant Channel to the west, the lower slope part of PD to the east and the transition to flat geomorphology to the north and south. This area is characterized by complex geomorphology includes folds, faults, ridges, seepage. Large pockmark and active gas and brine seepage have been documented in this area with their accompanying ecological hotspots.

Sediment Waves. Delineated by the eastern flood plains of Levant Channel to the west, the 1250 m isobath to the east and the transition from sediment waves to folds in the south. This area is characterized by large (>1km in width) sediment waves, associated with prominent ESE to WNW sediment transport features.

Main Deep-Sea Fan. Delineated to the north by the Levant Channel flood plains, to the south by the 1250m isobath (gas presence) and to the east by the foothills of the PD (Palmahim A). This zone is characterized by prevalent deep-water channels, over-bank deposits, deep-water fans, folds and faults are also present.

Southern Deep-Sea Fan. Delineated to the north by the 1250m isobath (range of gas presence) and to the east by the base of slope. Part of the Deep-Sea Fan marked by prevalent presence of pockmarks and indications of active seepage. Of these most notable is the large Gal-C pockmarks, where active seepage and deep-water benthic fauna were observed. This area hosts the bulk of the deep-water fans and over-bank deposits as well as exhibits a denser faulting system relative to other parts of the Deep-Sea Fan.

Deep Plain - Delineated by the eastern flood plains of Levant Channel to the west, the 1250 isobath to the east and the sediment wave domain to the north. This is a relatively flat area without strong complex geomorphology features, the main features present are gentle folds (in the western part of his area) and some faults (in the eastern part of the area).

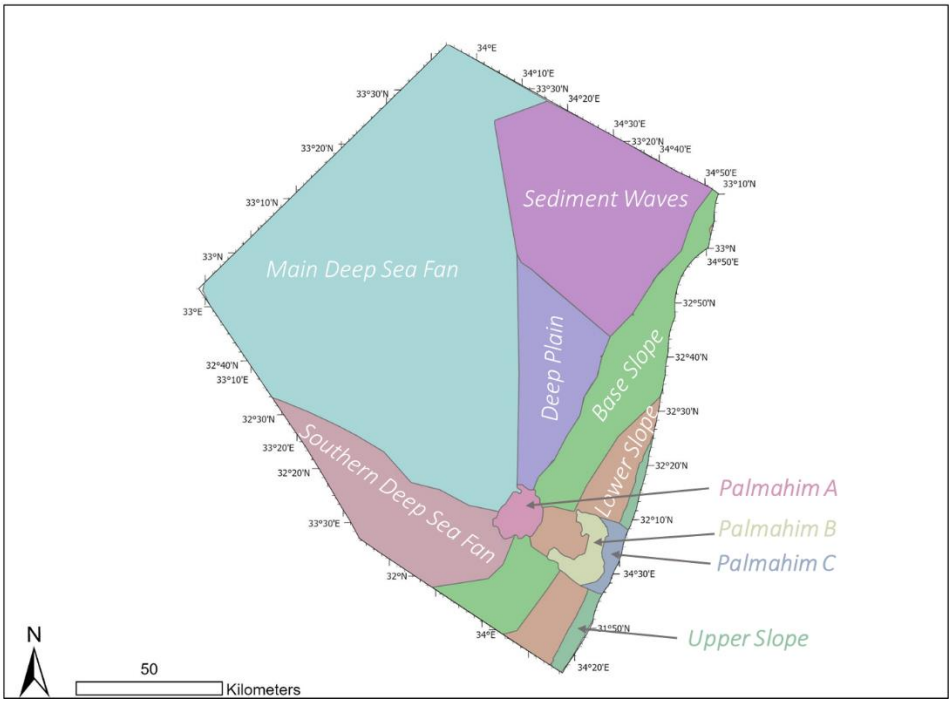

Figure 8. Geomorphic domains in the EEZ.

Sediments analysis demonstrates that carbonate detritus in the sediment originating from pelagic and benthic sources, weaken the correlation of grain size with the depth and distance from the coast. Notable in this respect is the significant contribution of carbonate to the sand fraction, and particularly in the deeper parts of the basin, indicating the biogenic source of most of the sand-size grains (Figure 9)

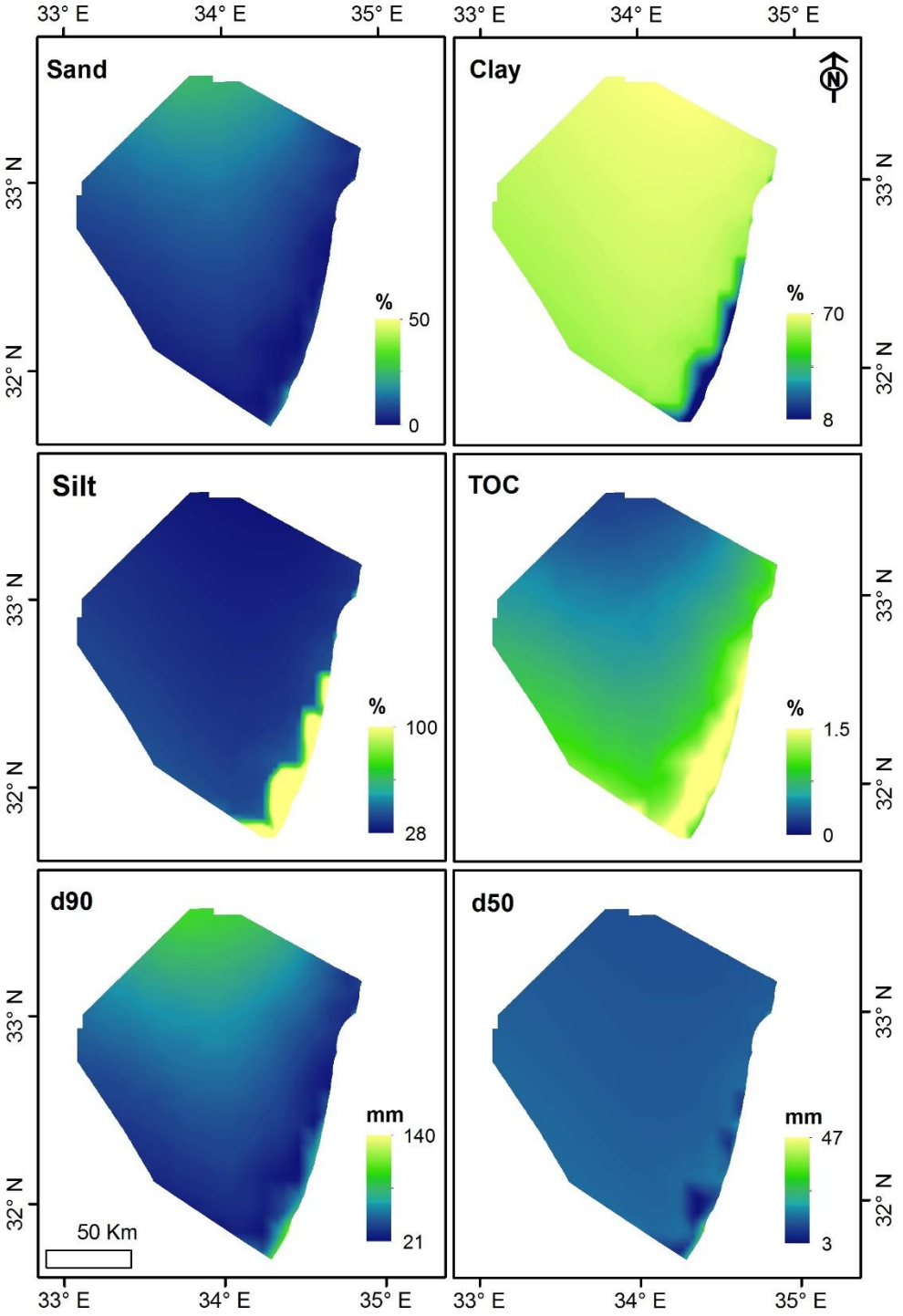

Figure 9. Sediments distribution in the EEZ. Sand = grain size of 63-2000µm; Silt = grain size of 8-63µm; Clay = grain size <8µm; TOC = total organic carbon - represents the organic matter in the sediments; d90 = 90th percentile of grain size distribution in sample; d50 = 50th percentile of grain size distribution in sample. The raw data used for the analysis was obtained from Elyashiv and Kruvi (2016).

In the cluster analysis of the biological data an optimal number of 14 clusters was selected (Figure 10).

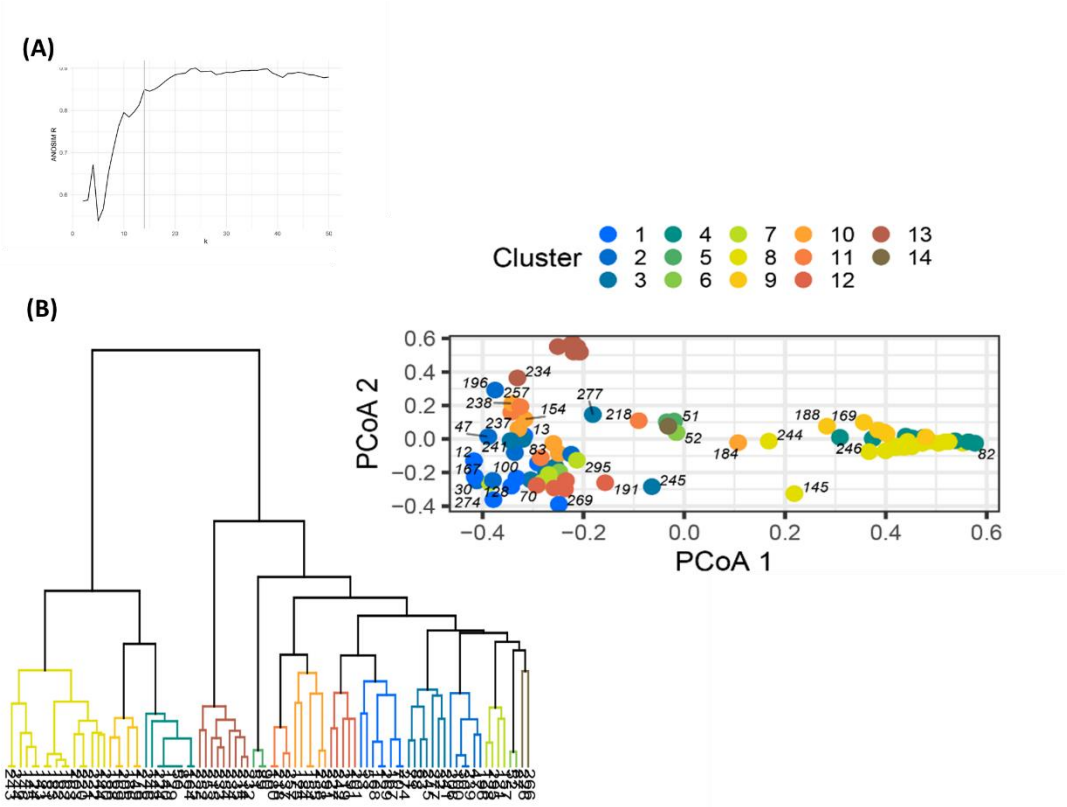

Figure 10. (A) Plot of ANOSIM test statistic R against *k* clusters. The vertical grey line represents the optimal *k* (=14) that was selected. (B) Dendogram showing hierarchical clustering of cells based on Simpson dissimilarity, colored by cluster, with inset PCoA plot showing the clustered cells in multidimensional ordinated space.

Some clusters showed strong geographical cohesiveness (e.g. 8, 13; Figure 11), whereas others were geographically extremely widespread (e.g. 1, 3, 4, 12).

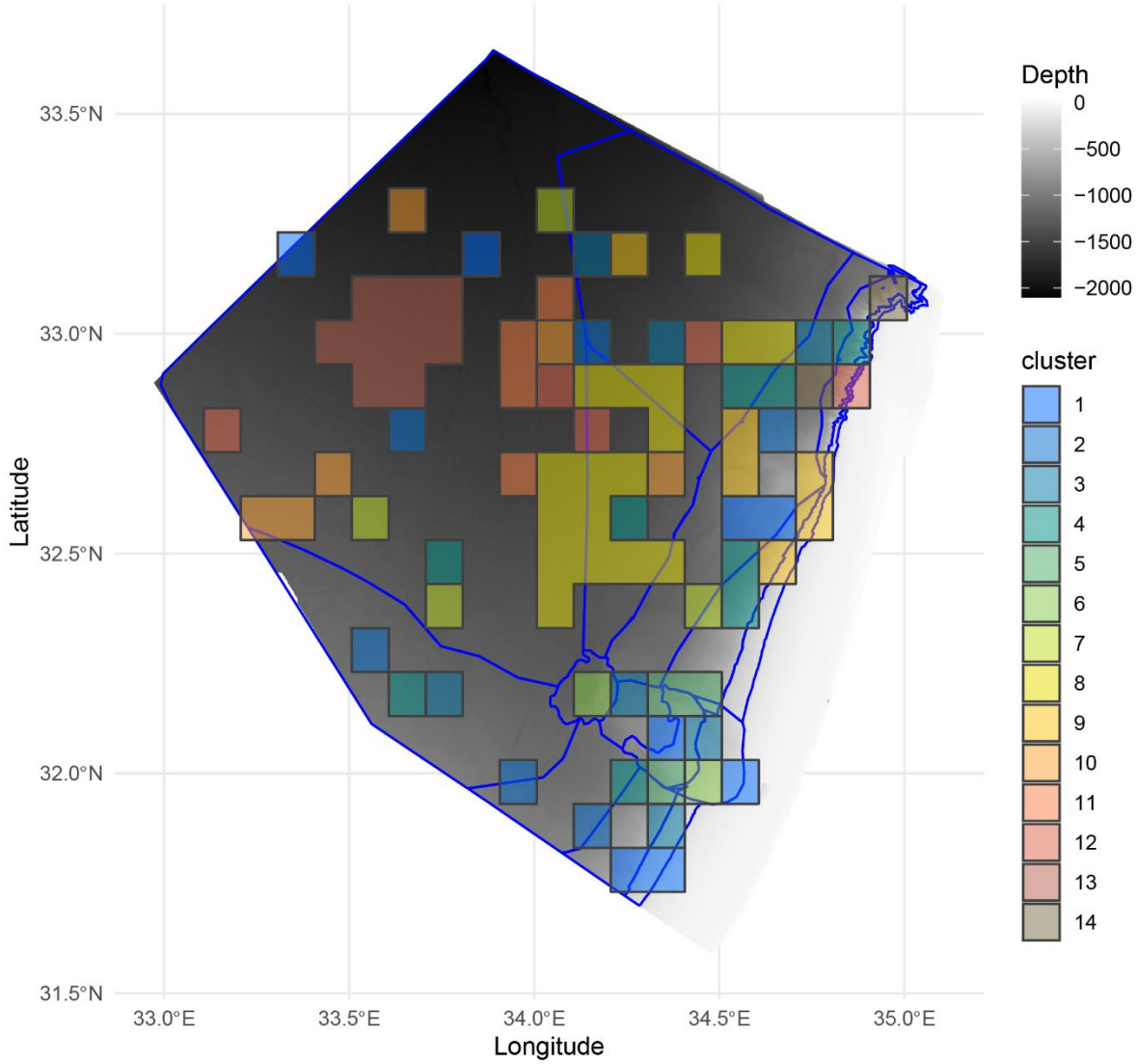

Figure 11. Map of 0.1*0.1 degree cells colored by clusters based on Simpson dissimilarity. Depth is shown in a greyscale gradient, with darker colors representing deeper seafloor, and blue lines denoting different geomorphological domains.

Biological assemblages were generated based on the results of the clustering analyses and through examination of unique faunal elements in different assemblages. Clusters were joined together or split apart to reflect unique faunal assemblages, which likely represent distinct ecological functions, and based on predicted dissimilarity according to the GDM. A final map of 5 biological assemblages was generated (Figure 12).

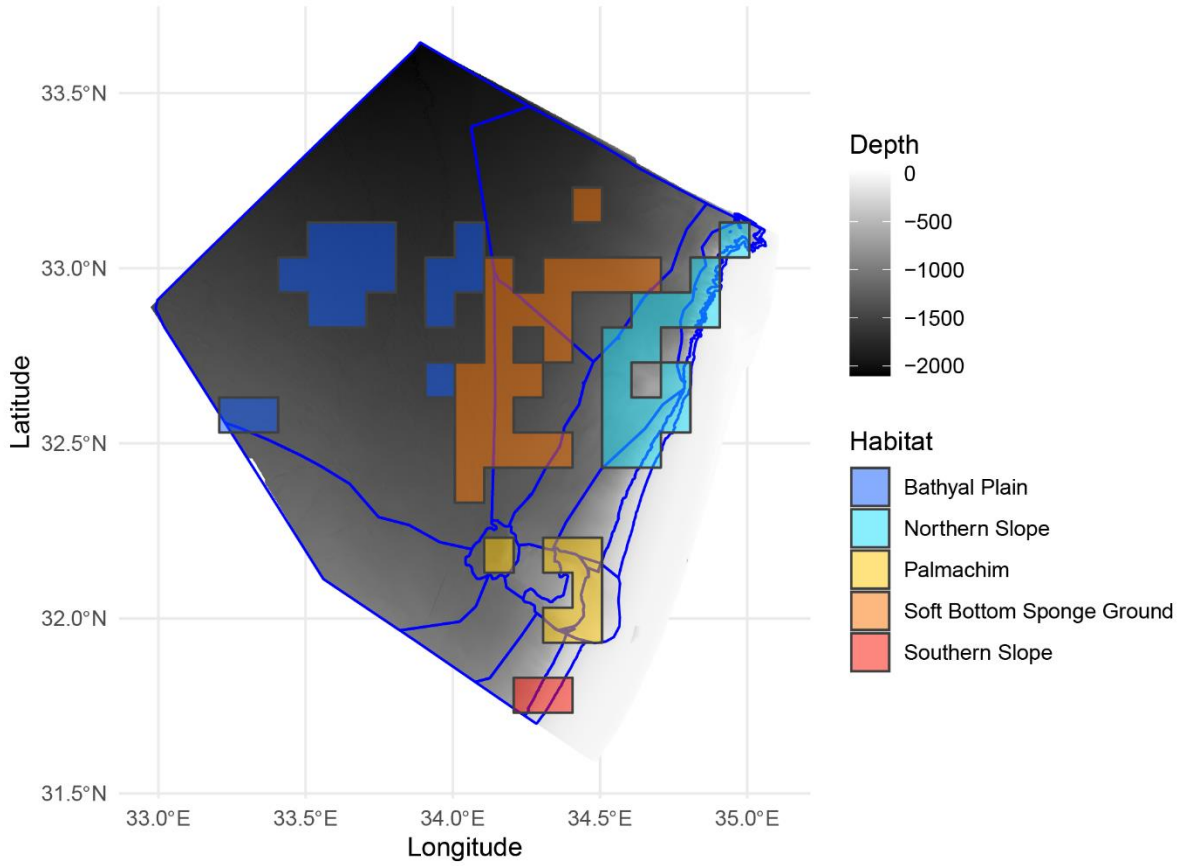

Figure 12. Map of distinct representative biological assemblages, based on clustering done on 0.1*0.1 degree cells. Depth is shown in a greyscale gradient, with darker colors representing deeper seafloor, and blue lines denoting different geomorphological domains.

Notably, some cells are not represented in the final map, particularly in clusters 1, 3 and 4 from the southern and south-western areas of the EEZ. The clusters there are generally comprised of small assemblages with extremely low percentages of unique taxa. Many of the sampled taxa have poorly-resolved taxonomic resolution and are lacking much ecological knowledge, but are nevertheless likely wide-spread. These cells were therefore omitted, since they likely represent dubious clustering due to sampling issues, and there is high uncertainty around which assemblage, if any, they represent.

Due to this, and general lack of sampling, the current assemblage classification of much of the southern and northern EEZ remain unknown. However, the GDM predictions (Figure 13) suggest that the southern EEZ may be similar in faunal composition to much of the base slope, while the northern EEZ may be entirely unique.

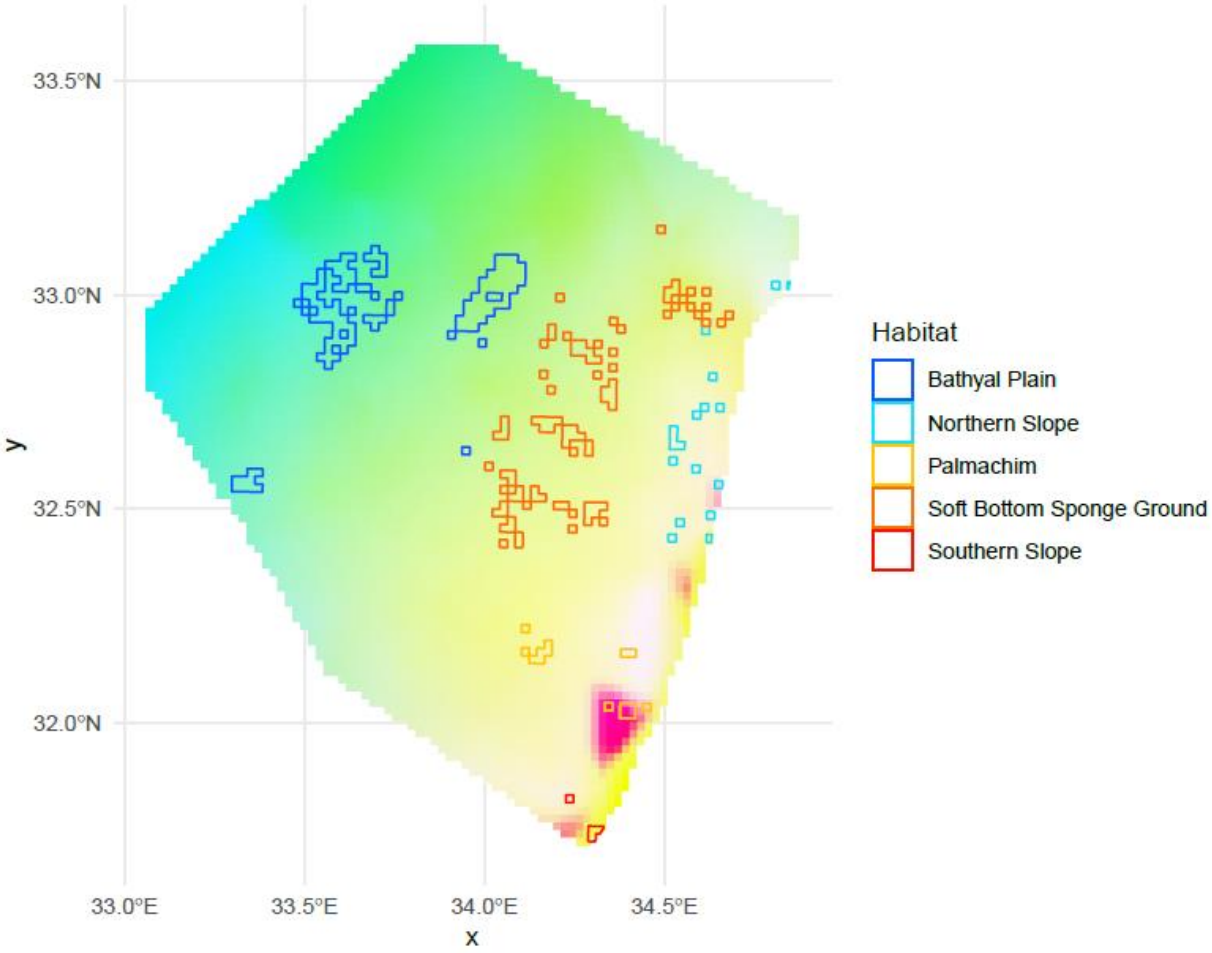

Figure 13. Map of predicted biological composition from a Generalized Dissimilarity Model (GDM). Similar colors represent similar predicted faunal compositions. Representative assemblages are overlayed in 2 km cells in which observed samples exist.

Biological assemblage description

1. **Northern Slope:**

Defined by the presence of taxa that are associated both with shallow and deep water, as well as taxa associated with both soft and hard substrates. Unique elements include endangered species (*Tonna galea*) and unidentified soft corals. The northernmost edge of the area of the assemblage might contain a unique assemblage of hard-substrate associated taxa (*Scyllarides latus, Centrostephanus longispinus*, etc.), but sampling is too scarce to say definitively at this moment. Many of the taxa present in this assemblage are also common in shallower habitats and there is a large presence of benthopelagic taxa. The extremely low ratio of wide-spread taxa also suggests that this assemblage might be comprised of several distinct habitats with unique assemblages.

Geomorphological domains: Upper Slope, Lower Slope, Base Slope, Sediment Waves.

Location: North-East.

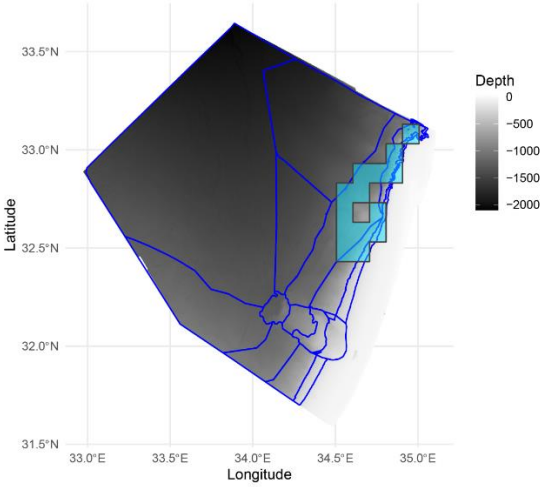

Figure 14. Map of the Northern Slope biological assemblage. Depth is shown in a greyscale gradient, with darker colors representing deeper seafloor, and blue lines denoting different geomorphological domains.

Table 6. Northern Slope biological assemblage description	
Wide-Spread Taxa (found in >50% cells)	*Polycheles typhlops*
% Wide-Spread Taxa	0.7%
% Unique Taxa	37.1%
Potential Indicator Taxa	None
Functional entities (fe number as in Table 1:Number of taxa in the assemblage)	fe_1: 37 fe_4: 15 fe_2: 13 fe_6: 12 fe_3: 9 fe_5: 7 fe_7: 7 fe_10: 5 fe_8: 4 fe_9: 4 fe_11: 1
Functional over-redundancy	deposit feeders & carnivores
SIMPER (taxa that contribute to at least 70% difference between this and the 4 other assemblages)	*Aristaeomorpha foliacea, Galeodea echinophora*

2. **Southern Slope:**

Defined by the presence of unique taxa suggestive of possible chemosynthetic communities and soft substrates. Multiple specimens of an unidentified species of *Cossura* are present, and some species in the genus are known to be chemosymbionts. In addition, presence of *Thyasira flexuosa* and *Eriopisa elongata* was observed.

Geomorphological domains: Upper Slope, Lower Slope.

Location: South-East.

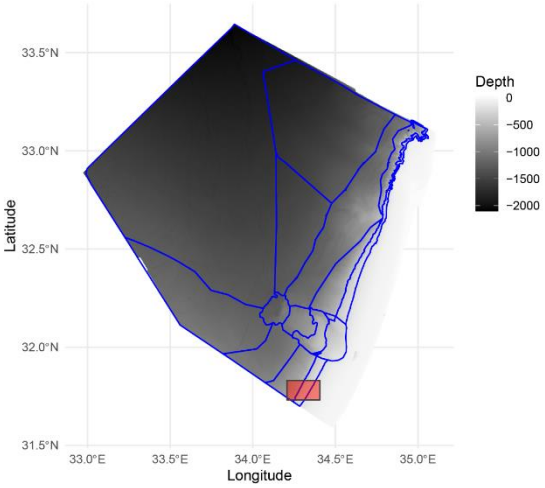

Figure 15. Map of the Southern Slope biological assemblage. Depth is shown in a greyscale gradient, with darker colors representing deeper seafloor, and blue lines denoting different geomorphological domains.

Table 7. Southern Slope biological assemblage description	
Wide-Spread Taxa (found in >50% cells)	*Ancistrosyllis groenlandica, Aricidea (Acmira) lopezi, Aricidea (Aedicira) sp., Aricidea (Allia) antennata, Aricidea (Allia) monicae, Aricidea (Aricidea) wassi, Brania sp., Carangoliopsis spinulosa, Caudofoveata sp., Clitellata sp., Cossura sp., Desmosomatidae sp., Ennucula tenuis, Exogone sp., Gallardoneris sp., Glycera lapidium, Heteronemertea sp., Hyperiidea sp., Levinsenia sp., Litocorsa stremma, Mediomastus sp., Monticellina sp., Nassarius elatus, Nephtyidae sp., Notomastus sp., Ophiuroidea sp., Palaeonemertea sp., Panthalis oerstedi, Podarkeopsis sp., Praxillella gracilis, Prionospio sp., Pseudotanais sp., Spiophanes sp., Sternaspis scutata.*
% Wide-Spread Taxa	41.5%
% Unique Taxa	24.4%
Potential Indicator Taxa	*Aricidea (Acmira) lopezi, Aricidea (Aedicira) sp., Ennucula tenuis, Litocorsa stremma, Monticellina sp., Nassarius elatus*
Functional entities (fe number as in Table 4:Number of	fe_1: 21 fe_3: 19 fe_2: 10 fe_9: 3 fe_6: 2 fe_12: 1

taxa in the assemblage)	fe_4: 1 fe_5: 1 fe_7: 1
Functional over-redundancy	infauna
SIMPER (taxa that contribute to at least 70% difference between this and the 4 other assemblages)	*Abyssoninoe sp., Ancistrosyllis groenlandica, Anobothrus gracilis, Aricidea (Acmira) lopezi, Aricidea (Aedicira) sp., Aricidea (Allia) antennata, Aricidea (Allia) monicae, Aricidea (Aricidea) wassi, Brania sp., Carangoliopsis spinulosa, Caudofoveata sp., Clitellata sp., Cossura sp., Desmosomatidae sp., Edwardsiidae sp., Ennucula tenuis, Exogone sp., Gallardoneris sp., Glycera lapidium, Heteronemertea sp., Hyperiidea sp., Levinsenia sp., Litocorsa stremma, Mediomastus sp., Monticellina sp., Nassarius elatus, Nephtyidae sp., Ophiuroidea sp., Palaeonemertea sp., Panthalis oerstedi, Podarkeopsis sp., Praxillella gracilis, Prionospio sp., Pseudotanais sp., Spiophanes sp., Sternaspis scutata*

3. <u>Palmahim:</u>

A collection of several highly unique habitats and communities in close spatial proximity, as exemplified by the lack of wide-spread taxa that are common throughout the entire area of the assemblage. Most prominently coral gardens (mostly in the region of Palmahim B), and chemosynthetic tube worms (*Lamellibrachia anaximandri* and unident. sp. ["chemo tube worms"]), and other chemosynthetic taxa (*Lurifax vitreus*, Possibly *Sigambra* sp.) in cold seeps (mostly in the region of Palmahim A).

Geomorphological domains: Palmahim A, Palmahim B, Palmahim C.

Location: South-East.

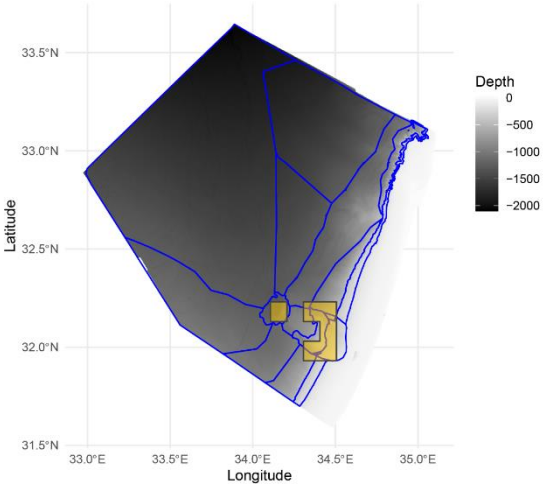

Figure 16. Map of the Palmahim biological assemblage. Depth is shown in a greyscale gradient, with darker colors representing deeper seafloor, and blue lines denoting different geomorphological domains.

Table 8. Palmahim biological assemblage description

Wide-Spread Taxa (found in >50% cells)	None
% Wide-Spread Taxa	0%
Unique Taxa (only found in this assemblage; taxon names as appear in data source)	*Anekes paucistriata, Antipathes dichotoma, Calliax lobata, Callogorgia verticillata, Chemo tube worms, Clelandella miliaris, Crinoidea sp., Ennucula corbuloides, Epizoanthus sp., Funiculina quadrangularis, Isidella elongata, Isorropodon perplexum, Laeviphitus verduini, Lamellibrachia anaximandri, Leiopathes sp., Leptognathiella DS#2, Leptognathiopsis sp., Lucinoma kazani, Lurifax vitreus, Myrtea amorpha, Mytilidae sp., Oediceroides pilosus, Parantipathes sp., Pleurotomella eurybrocha, Protanaissus sp., Putzeysia wiseri, Solatisonax alleryi, Swiftia pallida, Taranis moerchii, Thyasira biplicata, Viminella flagellum, Waisiuconcha corsellii, Xylophaga dorsalis, Yoldiella nana, Yoldiella striolata.*
% Unique Taxa	38.9%
Potential Indicator Taxa	None
Functional entities (fe number as in Table 4:Number of taxa in the assemblage)	fe_2: 18 fe_1: 13 fe_3: 8 fe_5: 8 fe_4: 7 fe_6: 7 fe_12: 3 fe_9: 3 fe_13: 2
Functional over-redundancy	infaunal filter feeders & deposit feeders
SIMPER (taxa that contribute to at least 70% difference between this and the 4 other assemblages)	*Antipathes dichotoma, Callogorgia verticillata, Crinoidea sp., Funiculina quadrangularis, Isidella elongata, Leiopathes sp., Parantipathes sp., Swiftia pallida*

4. <u>Soft Bottom Sponge Ground:</u>

Vastly distributed biological assemblage defined by unique assemblages of sponges associated with soft substrates, most prominently *Rhizaxinella shikmonae*, unique to this assemblage, and wide-spread throughout. Unlike most deep-sea habitats where the most dominant fauna are infaunal deposit feeders, this assemblage is extremely rich in benthic filter feeders and carnivores. The widespread sponges in this habitat may act as habitat builders and thus promote biodiversity.

Geomorphological domains: Sediment Waves, Deep Plain, Main Deep-Sea Fan.

Location: Centre.

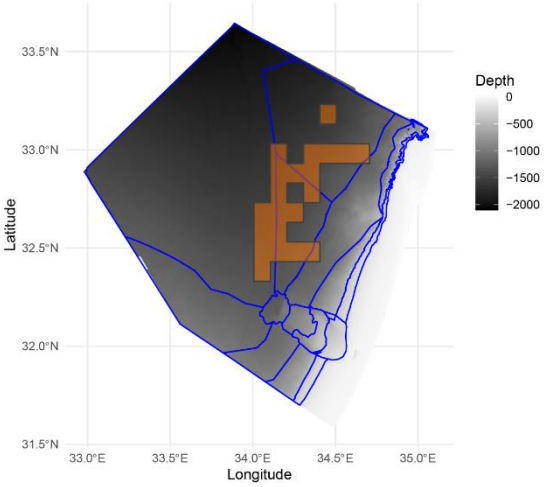

Figure 17. Map of the Soft Bottom Sponge Ground biological assemblage. Depth is shown in a greyscale gradient, with darker colors representing deeper seafloor, and blue lines denoting different geomorphological domains.

Table 9. Soft Bottom Sponge Ground biological assemblage description	
Wide-Spread Taxa (found in >50% cells)	Aristeus antennatus, Geryon longipes, Polycheles typhlops, Rhizaxinella shikmonae
% Wide-Spread Taxa	7.4%
% Unique Taxa	35.6%
Potential Indicator Taxa	Rhizaxinella shikmonae
Functional entities (fe number as in Table 4:Number of taxa in the assemblage)	fe_1: 9 fe_3: 7 fe_2: 6 fe_4: 6 fe_8: 6 fe_5: 3 fe_10: 2 fe_6: 2 fe_7: 2 fe_9: 1
Functional over-redundancy	filter feeders and carnivores
SIMPER (taxa that contribute to at least 70% difference between this and the 4 other assemblages)	*Aristeus antennatus, Benthonella tenella, Geryon longipes, Polycheles typhlops, Rhizaxinella shikmonae, Yoldiella micrometrica*

5. **Bathyal Plain:**

Characterised by rich infaunal assemblages of polychaete worms, mostly from the families Glyceridae (carnivores), and Capitellidae and Spionidae (deposit feeders). Worth mentioning is the presence of *Phoronis* sp, the only recorded representative of the phylum Phoronida (horseshoe worms) in the EEZ. Comprised of several distinct clusters (10, 11, 12), but joined together based on similar functional characteristics, similar predicted composition based on GDM (Figure. 12), and unequal sampling effort throughout the EEZ likely contributing to artificial separation between clusters. However, some differences likely still exist, and distribution of represented taxa may be patchy, as is also suggested by the GDM (Figure 13).

Geomorphological domains: Main Deep-Sea Fan.

Location: West.

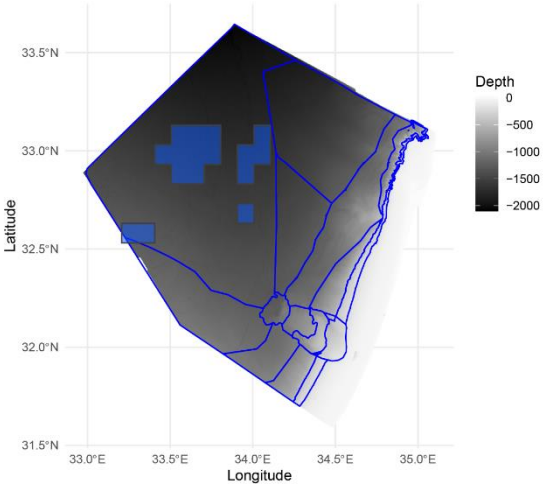

Figure 18. Map of the Bathyal Plain biological assemblage. Depth is shown in a greyscale gradient, with darker colors representing deeper seafloor, and blue lines denoting different geomorphological domains.

Table 10. Bathyal Plain biological assemblage description	
Wide-Spread Taxa (found in >50% cells)	*Aphelochaeta sp., Clitellata sp., Nannastacidae sp., Notomastus sp., Polycirrinae sp., Scolelepis sp., Spiochaetopterus sp.*
% Wide-Spread Taxa	4.7%
% Unique Taxa	35.3%
Potential Indicator Taxa	*Scolelepis sp.*
Functional entities (fe number as in Table 4:Number of taxa in the assemblage)	fe_1: 30 fe_3: 22 fe_2: 9 fe_4: 5 fe_6: 5 fe_11: 4 fe_7: 3 fe_5: 2 fe_8: 2

	fe_14: 1 fe_9: 1
Functional over-redundancy	infaunal deposit feeders & carnivores
SIMPER (taxa that contribute to at least 70% difference between this and the 4 other assemblages)	*Aphelochaeta sp., Glycera fallax, Leptochelia tanykeraia, Nannastacidae sp., Polycirrinae sp., Scolelepis sp., Spiochaetopterus sp., Stylochidae sp., Typhlotanais angstromensis*

Uncertainty in biological assemblages composition

Overall, Palmahim had the highest relative certainty score, followed by Bathyal Plain and Northern Slope (tied for second and third), Southern Slope, and finally Soft Bottom Sponge Ground with the lowest relative certainty score (Table 11). However, assemblages varied in which metric most contributed to their certainty. Palmahim ranked highly in almost all metrics, being a well-sampled, well-studied area with many endemic taxa that are widespread throughout the assemblage. The Bathyal Plain and Northern Slope both ranked around the middle in most metrics, but ranked the highest in endemism metrics – Bathyal Plain in having the highest proportion of its taxa's ranges included within the area of assemblage (Annex 1 - Figure A9A), and Northern Slope in having the highest proportion of endemic taxa. Similarly, Southern Slope and Soft Bottom Sponge Ground ranked lowest in certainty for different reasons – Southern Slope has the highest sampling density (Annex 1 - Figure A10) and commonality index (Annex - Figure A9B) but lowest endemism scores, whereas Soft Bottom Sponge Ground ranks highest in taxonomic resolution (Annex 1 - Figure A9C), but lowest on sampling density (Annex - Figure A10).

Table 11. Certainty scores for the different biological assemblages. For each metric the rank order is given in parentheses, ranging from 1 (lowest) to 5 (highest). The certainty score is an unweighted average of the five rank orders.

Assemblage	**Mean AOO/Habitat**	**Mean Habitat/AOO**	**Sampling Density**	**Mean Taxonomic Resolution**	**% Endemic Taxa**	**Certainty**
Palmahim	48.9 (2)	4.36 (4)	1.50 (4)	4.87 (4)	41.1 (4)	3.6
Bathyal Plain	70.2 (5)	1.47 (3)	0.58 (3)	4.32 (1)	35.3 (3)	3
Northern Slope	58.1 (4)	0.79 (1)	0.33 (2)	4.49 (3)	42.0 (5)	3
Southern Slope	46.8 (1)	8.21 (5)	2.44 (5)	4.45 (2)	24.4 (1)	2.8
Soft Bottom Sponge Ground	53.7 (3)	0.99 (2)	0.19 (1)	4.89 (5)	35.2 (2)	2.6

Foraminiferous unique assemblage*						1

* Score for Foraminiferous unique assemblage is qualitative, see Methods.

Weighted average (giving higher weight to sampling density and taxonomic identification, or to endemism metrics) changed the certainty scores but the relative ordering of biological assemblages from least to most certain did not.

Detailed results of the clustering analysis and biological assemblages' characterization are available in Annex 1 and Appendix 1.

Delineation of representative benthic ecological units in the EEZ resulted in 21 units (Figure 19). It is suggested that some of these units can be merged based on experts' opinion (see Discussion section).

Nine sampling points used by Rubin-Blum et al. (2022) for characterization of benthic microbial communities in the sediment intersect six different ecological units in: Unknown upper-slope, Unknown lower-slope, Unknown base-slope, Sponge ground sediment waves, Unknown sediment waves, and Unknown main deep sea fan. Generally, microbial diversity decreases with water depth. Ammonia-oxidizing archaea, aerobic heterotrophs, and saprotrophic fungi are dominant is all the above units. Ecological units along the continental slope are also characterized by presence of anaerobic heterotrophs and sulfate-reducing bacteria. Cluster analysis of the microbial communities reveal different pattern of diversity gradient between the northern and southern slope. Further monitoring of the bacterial communities in the different ecological units can refine units boundaries and characterization (see discussion section for recommendation).

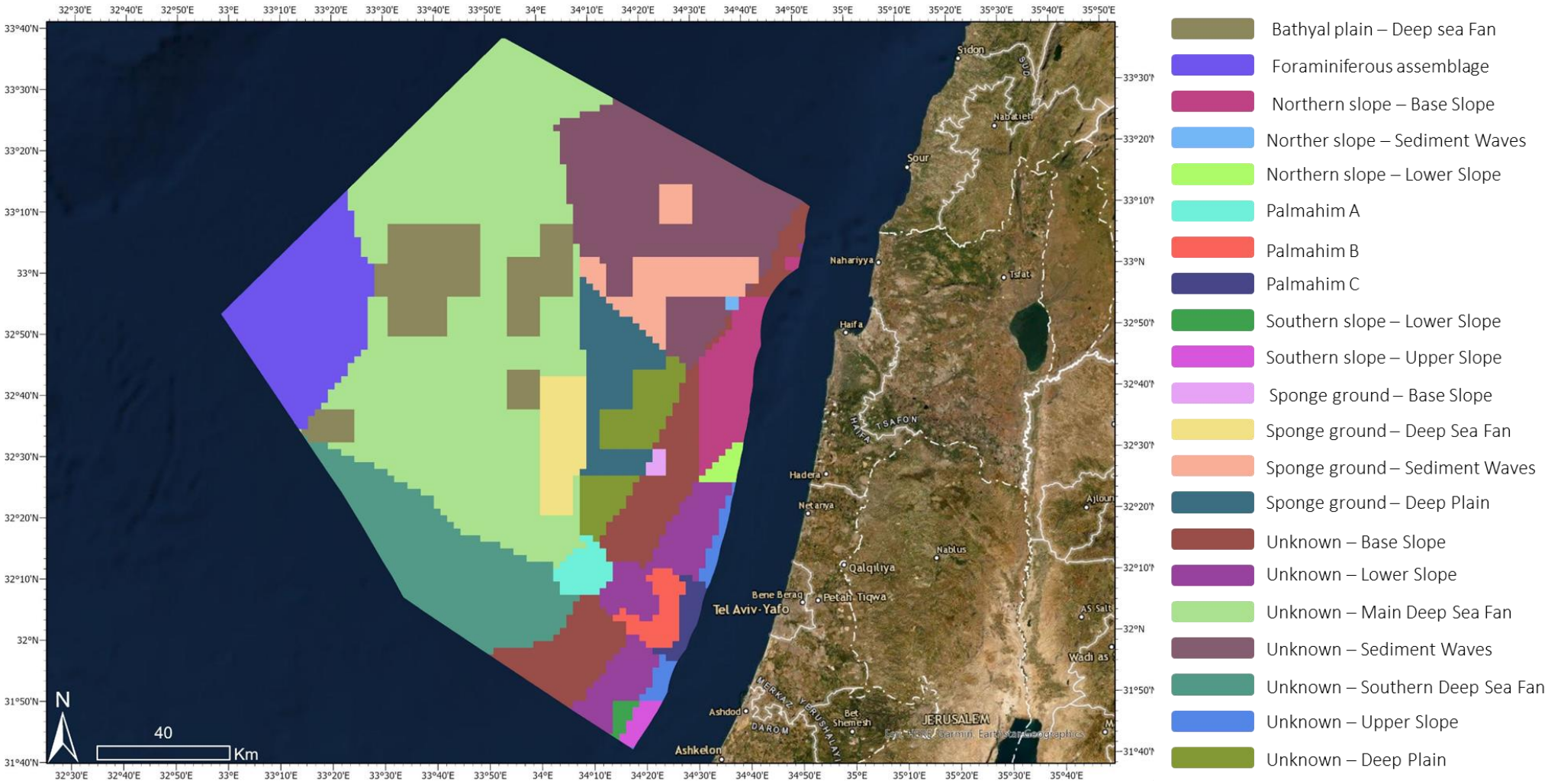

Figure 19. Representative benthic ecological units in the Israeli EEZ. Unit name is a combination of the biological assemblage and the geomorphic domain. "Unknown" refers to units with unknown biological assemblages

Unique benthic habitats

The results of the six different types of SDMs (GLM, GAM, CART, RF, BRT, and MaxEnt) for each indicator species are available in Appendix 2. Models validation using the 30% test set demonstrate that all SDMs performed extremely well for all nine indicator species (all had AUC values >0.8, and most over 0.95). For most taxa, committee average was the best ensemble model (algorithm used for models aggregation, see Table 12), with the exceptions of Chemosynthetic tube worms and *Isidella elongata* (both mean probability), and *Lamelliabrachia anaximandri* and *Rhizaxinella shikmonae* (both median probability). The best ensemble models all had AUC values >0.9, and TSS values >0.8, and most (apart from the model for *Rhizaxinella shikmonae*) explained a large proportion of deviance in the test set (Table 12).

Table 12. Summary table of the best performing ensemble model for each taxon. Listed are the algorithm used to construct the ensemble model, the area under the ROC curve (AUC), the sum of sensitivity and specificity (TSS), and the deviance explained (D^2).

Taxon	**Algorithm** (best ensemble model)	**AUC**	**TSS**	**D^2**	**Optimal Threshold**	**VME**
Antipathes dichotoma	Committee Average	1.00	1.00	0.97	0.67	Coral Gardens
Chemosynthetic tube worms	Mean Probability	0.99	0.96	0.84	0.08	Cold Seeps
Funiculina quadrangularis	Committee Average	1.00	1.00	0.97	0.83	Sea Pen Fields
Isidella elongata	Mean Probability	1.00	0.97	0.87	0.04	Coral Gardens
Lamellibrachia anaximandri	Median Probability	1.00	1.00	0.87	0.12	Cold Seeps
Rhizaxinella shikmonae	Median Probability	0.92	0.86	0.22	0.02	Soft Bottom Sponge Grounds
Swiftia pallida	Committee Average	1.00	0.99	0.88	0.58	Coral Gardens
Thyasira flexuosa	Committee Average	1.00	1.00	0.64	0.75	Cold Seeps
Viminella flagellum	Committee Average	1.00	1.00	0.97	0.83	Coral Gardens

Based on the ensemble models, predicted probabilities for VMEs were generated (Figure 20). Cold Seeps are predicted to occur in widespread areas across the south-east of the EEZ and the base

slope, but with relatively low probability. Similarly, Coral Gardens are predicted to occur throughout the lower slope in the east of the EEZ with relatively low probability. Thus, these two VMEs likely extend beyond the Palmahim disturbance. Conversely, Sea Pen Fields are only predicted to occur in the Palmahim disturbance where direct observations of *Funiculina quadrangularis* have been made. Finally, the Soft Bottom Sponge Ground is predicted to occur over an extensive and geographically contiguous area in the north-east of the EEZ, with the highest predicted probability in the geomorphological domain Deep Plain.

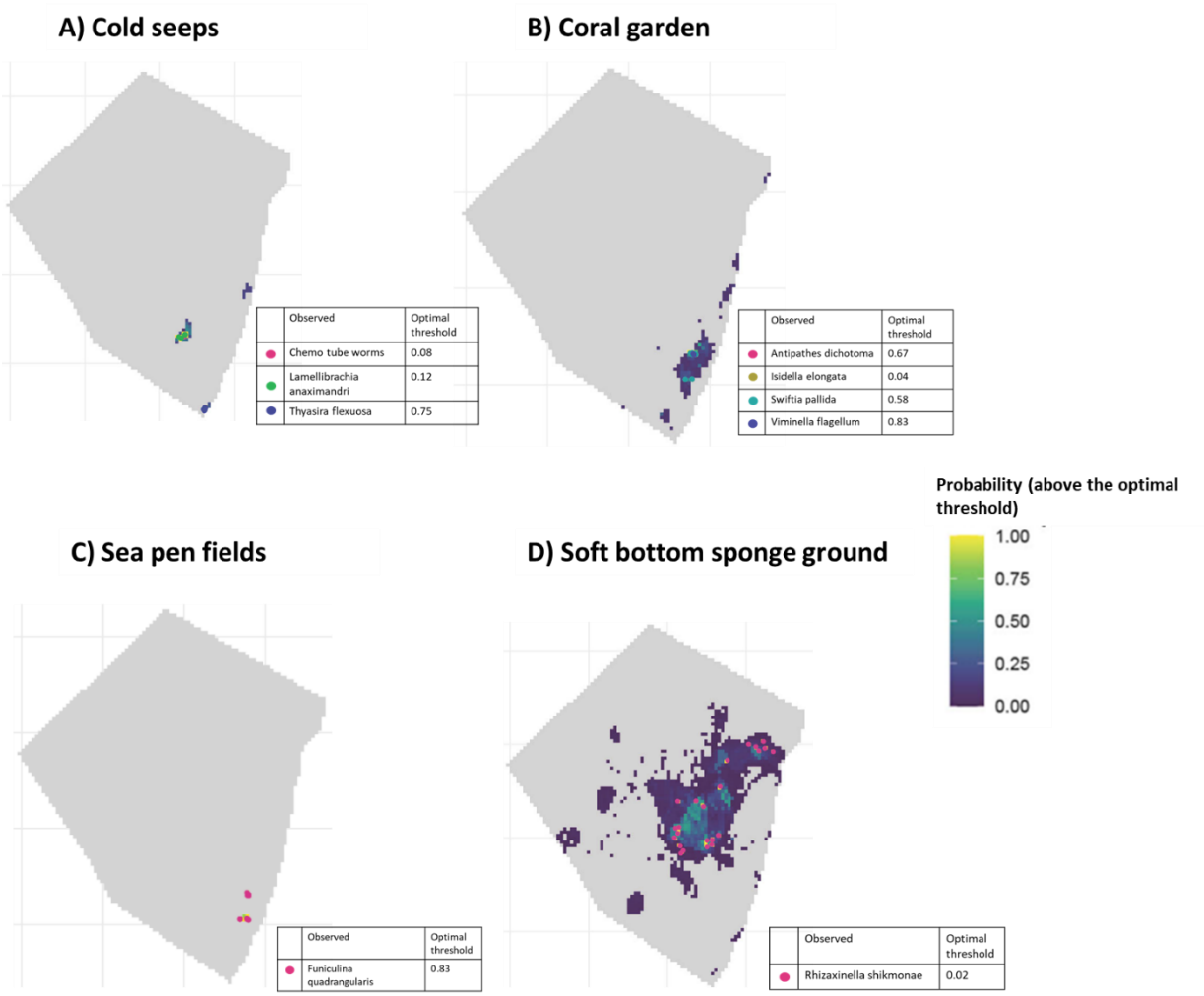

Figure 20. Predicted probabilities of four different VMEs. Grey areas are cells below the optimal threshold for all taxon SDMs, and thus the predicted probability for VME occurrence is 0. Colored dots and values of 1 represent direct observations of VME indicator taxa.

Based on observations and geomorphological feature, possible presence of indicator habitats for VMEs (rocks and pockmarks) is distributed along the continental slope base in several centers (Figure 21).

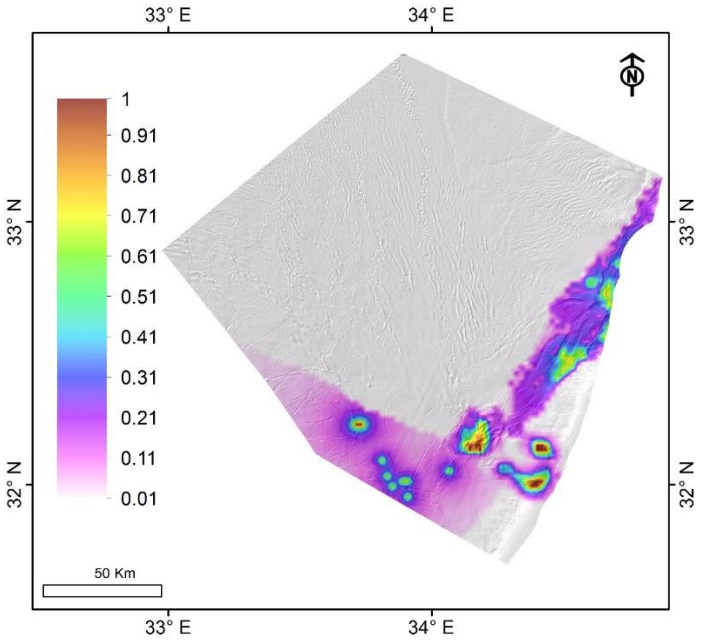

Figure 21. Gas seep pockmarks and rocky habitat distribution possibility based on seafloor observations and correlation with geomorphological features.

Discussion

The bioregionalization presented in this report demonstrates the multilevel habitats variability that exists in the area of the Israeli EEZ. It is the first attempt to provide ecological units classification for this area that is based on hierarchical scheme and that can capture environmental data of several scales, from broad biogeography to fine biological diversity contexts. Hierarchical classification clearly demonstrates the complexities of marine ecosystems while providing several scales of which conservation planning can relate to natural regions (Last et al. 2010, Harris 2020). The hierarchical approach that was used in this report, not only presents ecological units distribution, but also captures issues of spatial dynamics and uncertainties that should be considered in spatial prioritization for protection.

Despite previous conceptions regarding low faunal diversity in the EEZ, we used existing data on faunal distribution to demonstrate that variability do exist. Changing the old conception has significant planning implications as the entire basis for ecosystem-based planning and management in the area is changing. Therefore, the results of this work bind the promotion of significant spatial protection in the EEZ, and reconsidering future development there.

Additional efforts to fully characterize faunal and habitats distribution in the EEZ require further field sampling and analyses of existing, yet inaccessible data. Specific attention should be given to areas which were never before properly explored (e.g., the sediment waves domain, the southern deep-sea fan domain etc.). In addition, resources should be directed towards informative monitoring technics, such of microbial communities, which are recommended for identifying spatial biological trends and fundamental ecological processes (e.g., production). The methodology proposed here, allows for additional data to be easily incorporated and accounted for in plan's updates, that are recommended for bioregionalization and VME predictions improvements. We therefore recommend periodic update of the current work every 18-24 months, or less if significant amount of data becomes available. We also recommend that in the first update process, the cluster analysis will include sampling in the territorial waters (below 100 m) to better reflect the variability along the continental slope. Following the recommendation of the scientific committee who reviewed the current work, we also recommend assessing the sensitivity of the current results to various sampling methods and effort by including sampling frequency as weight for each grid-cell in the GDM.

The end products of this report to be used in spatial conservation prioritization, include maps of 21 representative benthic ecological units, and of 4 types of unique benthic habitats. Prior to using these products for prioritization, we suggest merging some representative benthic ecological units. The hierarchical classification scheme yielded 21 representative benthic ecological units, some which are very small. In most of these cases, this is due to biological assemblages that extend a short distance into neighboring geomorphological domain. For these cases, we suggest merging the small units with the rest of the area to form a continuous biological assemblage (Figure 22).

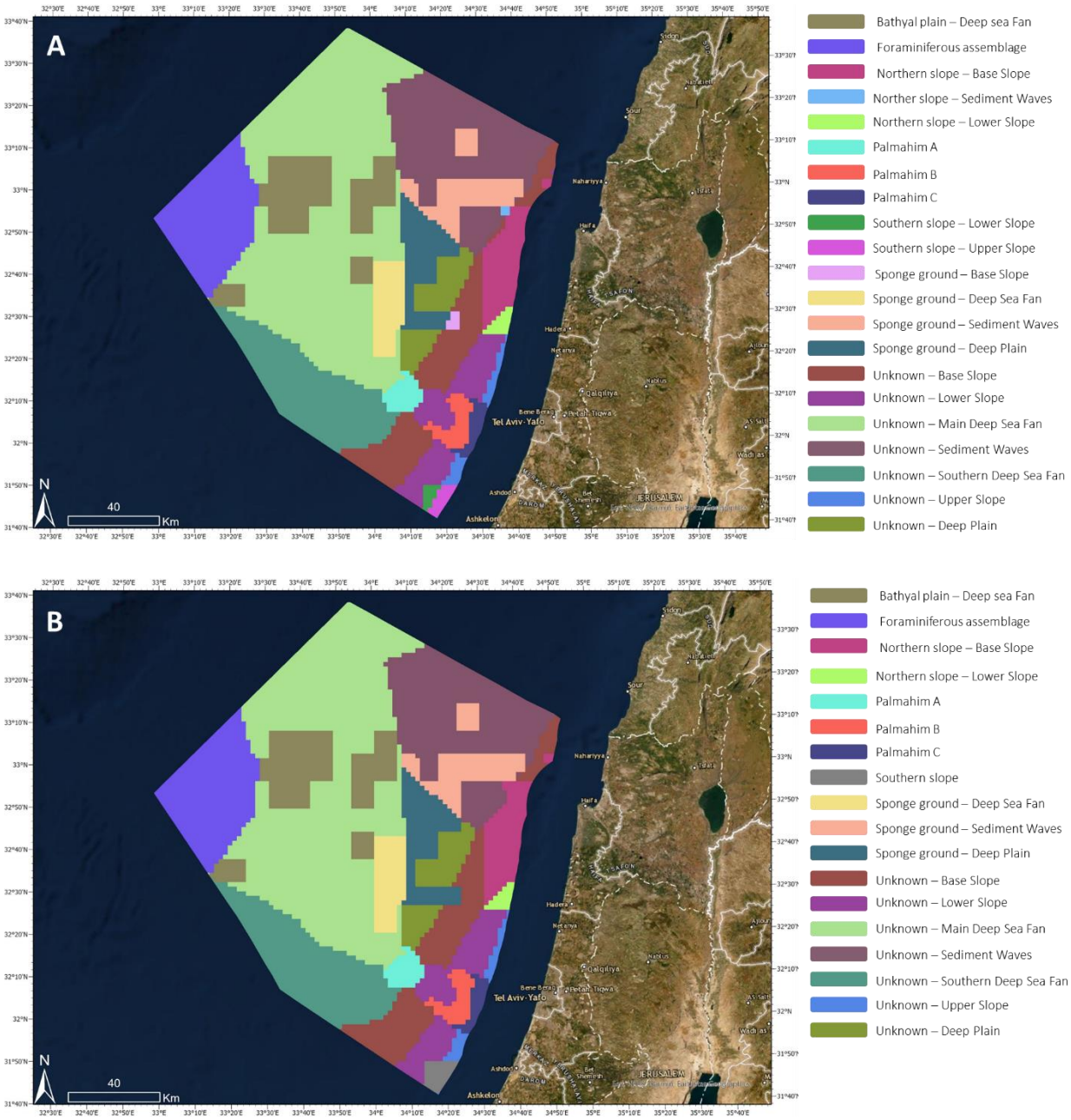

Figure 22. A. Representative benthic ecological units as suggested by the hierarchical classification. B. Suggested merging of representative benthic ecological units.

The spatial conservation prioritization requires conservation targets for each conservation feature, namely the representative ecological units and unique habitats. We suggest that conservation targets will be set based on the conservation value (representative / unique habitat), spatial extent, and level of certainty (Levin et al. 2015, Ceccarelli et al. 2021). Therefore, we suggest setting conservation targets while considering several rules of thumb following Ceccarelli et al. (2021) recommendations:

1. The total area for protection should cover at least 30% of the EEZ.
2. **For representative ecological units**:
   A. At least 20% of each unit should be targeted for protection[14].
   B. Conservation target of 100% should be applied to units with a total area of 1% or less of the EEZ.
   C. Conservation target of 50% should be applied to units with a total area of 5% or less of the EEZ.
   D. Conservation target of 30% should be applied to units with a total area of less than 10% but over 5% of the EEZ.
3. **For unique habitats**:
   A. Conservation target of 100% should be applied to areas where unique habitats were observed (certainty = 1). Supporting this target, is the fact that most of the species observed in unique habitat in the EEZ are declared protected natural assets in Israel (e.g., Cnidaria, Porifera).
   B. Conservation target of 100% should be applied to areas where unique habitats were indicated (by species distribution model) and have a total area of 1% or less of the EEZ.

In addition to the spatial targets, the conservation prioritization is intended to consider additional environmental and ecological variables such as connectivity, envisioned climate change impacts, as well as socioeconomic variables. Specific desirable connectivity is with MPAs in the territorial water that can create continuous protection over the continental slope that is considered highly variable and related to major transport dynamics to the deep sea. We therefore recommend that the prioritization will include scenarios with and without the MPAs in the territorial waters. We also recommend that the prioritization will promote spatial protection of mosaic of ecological units rather than a single MPA per unit to account for the uncertainty of species distribution and their movement in space.

The proposed conservation targets are listed in Table 13, including scientific committee recommendations for adjustments.

Table 13. Suggested conservation targets for conservation features in spatial conservation prioritization

Feature type	Conservation feature	Total area/% of EEZ (km^2/%)	Max. Level of certainty (0-1 scale)*	Conservation target (% of area for protection) **	Remarks

[14] From Ceccarelli et al. (2021): "*The best available science informs that at least 20–30% of each marine bioregion should be included in no-take areas, especially if aiming to protect species with lower reproductive output or delayed maturation (e.g., many large offshore and deep-water species), or in areas that host diverse, unassessed, or poorly regulated fisheries, as is common offshore*"

Representative benthic ecological units	Bathyal plain – Deep-Sea Fan	1592/7.0	0.6	30%	GDM results suggest that the unit is not significantly different from it surrounding and therefore reduced target of **20% is recommended**
	Foraminiferous assemblage	1908/8.4	0.2	30%	
	Northern Slope - Base Slope	760/3.3	0.6	50%	
	Northern slope- Lower Slope	100/0.4	0.6	100%	
	Palmahim A	216/0.9	0.72	100%	High certainty and limited distribution
	Palmahim B	248/1.0	0.72	100%	High certainty and limited distribution
	Palmahim C	180/0.7	0.72	100%	High certainty and limited distribution
	Southern Slope	176/0.7	0.56	100%	
	Sponge ground - Deep Sea Fan	536/2.3	0.52	50%	
	Sponge ground - Sediment Waves	784/3.4	0.52	50%	
	Sponge ground- Deep plain	840/3.7	0.52	50%	
	Unknown - Base Slope	1648/7.2	0	30%	
	Unknown - Lower Slope	996/4.3	0	50%	
	Unknown - Main Deep-Sea Fan	6920/30.5	0	20%	
	Unknown - Sediment Waves	2788/12.2	0	20%	
	Unknown - Southern Deep-Sea Fan	2104/9.2	0	30%	No known Biological assemblage in the domain

	Unknown - Upper Slope	228/1.0	0	100%	No known Biological assemblage in the domain after merging southern slope units
	Unknown- Deep plain	656/2.8	0	50%	Although unit is only 2.8% of EEZ, most of its domain is represented in known biological assemblage. Reduced target of **30% is recommended**
Unique benthic habitats	Soft bottom sponge ground	88/0.38	1	100%	Direct observations
	Soft bottom sponge ground	376/1.6	0.6	60%	Vast area Target match max probability
	Soft bottom sponge ground	2560/11.2	0.3	30%	Vast area Target match max probability. **Target can be reduced to 0%**
	Coral garden	24/0.1	1	100%	Direct observations
	Coral garden	516/2.2	0.7	70%	Limited area Target match max probability
	Sea pen field	28/0.1	1	100%	Direct observations
	Cold seeps	40/0.2	1	100%	Direct observations
	Cold seeps	388/1.6	0.7	70%	Limited area and relatively low certainty
	VME indicator habitat (rock and pockmarks)	116/0.5	1	100%	
	VME indicator habitat (rock and pockmarks)	356/1.5	0.7	50%	Vast area Target can be reduced for habitat indication compared with

					species indication
	VME indicator habitat (rock and pockmarks)	2260/10	0.4	30%	Vast area Target reduced for habitat indication compared with species indication Min. probability is 0.1
	Levant channel***	740/3.3	1	20%	

* For representative ecological units the certainty grade of 0-5 was transformed to 0-1 scale while 0 = 0 and 1= 5. For Unique benthic habitats distribution probability was used.

** Considering all conservation targets proposed in Table 13, the total area for protection will be at least 31% of the EEZ.

***Unique feature. A conservation target of 20% was suggested by experts in the consultation process

Following peer-review and experts' consultation, the products of this work will be used in spatial prioritization for conservation using the Marxan tool. In addition, the revised products will be used in Ecopath with Ecosim food-web model to examine ecosystem dynamic in relation to conservation and climate change scenarios.

References

Allee, R. J., M. Dethier, D. Brown, L. Deegan, R. G. Ford, T. F. Hourigan, J. Maragos, C. Schoch, K. Sealey, and R. Twilley. 2000. Marine and estuarine ecosystem and habitat classification.

Almogi-Labin, A., and O. Hyams-Kaphzan. 2016. בסמנים לתנאי קרקעית הים העמוק פורמיניפרה בנתונים

מול חופי ישראל. GSI, IOLR,.

Araújo, M. B., and M. New. 2007. Ensemble forecasting of species distributions. Trends in ecology & evolution **22**:42-47.

Araújo, M. B., R. G. Pearson, W. Thuiller, and M. Erhard. 2005. Validation of species–climate impact models under climate change. Global Change Biology **11**:1504-1513.

Baselga, A. 2010. Partitioning the turnover and nestedness components of beta diversity. Global Ecology and Biogeography **19**:134-143.

Baselga, A., and F. Leprieur. 2015. Comparing methods to separate components of beta diversity. Methods in Ecology and Evolution **6**:1069-1079.

Baselga, A., D. Orme, S. Villéger, J. De Bortoli, F. Leprieur, and M. Logez. 2022. betapart: Partitioning beta diversity into turnover and nestedness components. R Package 'betapart'. Version 1.5.6 **1**.

Ben Rais Lasram, F., F. Guilhaumon, C. Albouy, S. Somot, W. Thuiller, and D. Mouillot. 2010. The Mediterranean Sea as a 'cul-de-sac'for endemic fishes facing climate change. Global Change Biology **16**:3233-3245.

Bianchi, C., and G. Zurlini. 1984. Criteri e prospettive di una classificazione ecotipologica dei sistemi marini costieri italiani. Acqua aria **8**:785-796.

Bianchi, C. N. 2007. Biodiversity issues for the forthcoming tropical Mediterranean Sea. Hydrobiologia **580**:7-21.

Bland, L., D. Keith, R. Miller, N. Murray, and J. Rodríguez. 2017. Guidelines for the application of IUCN Red List of Ecosystems Categories and Criteria, version 1.1. International Union for the Conservation of Nature, Gland, Switzerland.

Castro-Insua, A., C. Gómez-Rodríguez, and A. Baselga. 2018. Dissimilarity measures affected by richness differences yield biased delimitations of biogeographic realms. Nature communications **9**:5084.

Ceccarelli, D. M., K. Davey, G. P. Jones, P. T. Harris, S. V. Matoto, J. Raubani, and L. Fernandes. 2021. How to Meet New Global Targets in the Offshore Realms: Biophysical Guidelines for Offshore Networks of No-Take Marine Protected Areas. Frontiers in Marine Science **8**.

Clarke, K. R. 1993. Non-parametric multivariate analyses of changes in community structure. Australian journal of ecology **18**:117-143.

Connor, D., N. Golding, P. Robinson, D. Todd, and E. Verling. 2006. UKSeaMap: The mapping of marine seabed and water column features of UK seas. Final report. Joint Nature Conservation Committee, Peterborough.

Cordes, E. E., D. O. B. Jones, T. A. Schlacher, D. J. Amon, A. F. Bernardino, S. Brooke, R. Carney, D. M. DeLeo, K. M. Dunlop, E. G. Escobar-Briones, A. R. Gates, L. Génio, J. Gobin, L.-A. Henry, S. Herrera, S. Hoyt, M. Joye, S. Kark, N. C. Mestre, A. Metaxas, S. Pfeifer, K. Sink, A. K. Sweetman, and U. Witte. 2016. Environmental Impacts of the Deep-Water Oil and Gas Industry: A Review to Guide Management Strategies. Frontiers in Environmental Science **4**.

Davies, C., and D. Moss. 1998. European Union Nature Information System (EUNIS) Habitat Classification. Report to European Topic Centre on Nature Conservation from the Institute of Terrestrial Ecology, Monks Wood, Cambridgeshire.[Final draft with further revisions to marine habitats.], Brussels: European Environment Agency.

Davies, C. E., D. Moss, and M. O. Hill. 2004. EUNIS habitat classification revised 2004. Report to: European environment agency-European topic centre on nature protection and biodiversity:127-143.

Dunstan, P. K., D. Hayes, S. Woolley, V. Allain, D. Leduc, A. Flynn, A. A. Rowden, and F. Stephanson. 2020. Bioregions of the South West Pacific Ocean. CSIRO, CSIRO, Australia.

Elith, J., S. J. Phillips, T. Hastie, M. Dudík, Y. E. Chee, and C. J. Yates. 2011. A statistical explanation of MaxEnt for ecologists. Diversity and distributions **17**:43-57.

Elyashiv, H., and O. Kruvi. 2016. מאפייני התפלגות גודל הגרגר בסדימנט. Geological Survey of Israel, IOLR,.

Fitzpatrick, M., K. Mokany, G. Manion, D. Nieto-Lugilde, S. Ferrier, and G. Started. 2022. gdm: Generalized Dissimilarity Modeling. R package version 1.5.

Franklin, J. 2010. Mapping species distributions: spatial inference and prediction. Cambridge University Press.

Gadol, O., G. Tibor, U. ten Brink, J. K. Hall, G. Groves-Gidney, G. Bar-Am, C. Hübscher, and Y. Makovsky. 2020. Semi-automated bathymetric spectral decomposition delineates the impact of mass wasting on the morphological evolution of the continental slope, offshore Israel. Basin Research **32**:1156-1183.

Gamliel, I., Y. Buba, T. Guy-Haim, T. Garval, D. Willette, G. Rilov, and J. Belmaker. 2020. Incorporating physiology into species distribution models moderates the projected impact of warming on selected Mediterranean marine species. Ecography **43**:1090-1106.

Greene, H. G., M. M. Yoklavich, R. M. Starr, V. M. O'Connell, W. W. Wakefield, D. E. Sullivan, J. E. McRea Jr, and G. M. Cailliet. 1999. A classification scheme for deep seafloor habitats. Oceanologica acta **22**:663-678.

Greenwell, B., B. Boehmke, J. Cunningham, and G. Developers. 2020. gbm: Generalized Boosted Regression Models. R package version 2.1.8.

Grorud-Colvert, K., J. Sullivan-Stack, C. Roberts, V. Constant, B. Horta e Costa, E. P. Pike, N. Kingston, D. Laffoley, E. Sala, and J. Claudet. 2021. The MPA Guide: A framework to achieve global goals for the ocean. Science **373**:eabf0861.

Guisan, A., W. Thuiller, and N. E. Zimmermann. 2017. Habitat suitability and distribution models: with applications in R. Cambridge University Press.

Guy-Haim, T., N. Stern, and G. Sisma-Ventura. 2022. Trophic ecology of deep-sea megafauna in the ultra-oligotrophic Southeastern Mediterranean Sea. bioRxiv.

Gvirtzman, Z., M. Reshef, O. Buch-Leviatan, G. Groves-Gidney, Z. Karcz, Y. Makovsky, and Z. Ben-Avraham. 2015. Bathymetry of the Levant basin: interaction of salt-tectonics and surficial mass movements. Marine Geology **360**:25-39.

Harris, P. T. 2007. Applications of geophysical information to the design of a representative system of marine protected areas in southeastern Australia. Pages 463-482 Mapping the Seafloor for Habitat Characterization. Geological Association of Canada St. John's, NL.

Harris, P. T. 2020. Biogeography, benthic ecology and habitat classification schemes. Pages 63-96 Seafloor geomorphology as benthic habitat. Elsevier.

Harris, P. T., and E. K. Baker. 2011. Seafloor Geomorphology as Benthic Habitat: GeoHab Atlas of seafloor geomorphic features and benthic habitats. Elsevier.

Hastie, T. 2022. gam: Generalized Additive Models. R package version 1.20.1.

Hastie, T., R. Tibshirani, J. H. Friedman, and J. H. Friedman. 2009. The elements of statistical learning: data mining, inference, and prediction. Springer.

Hijmans, R. J., S. J. Phillips, J. Leathwick, and J. Elith. 2021. dismo: Species Distribution Modeling. R package version 1.3-5.

Howell, K. L. 2010. A benthic classification system to aid in the implementation of marine protected area networks in the deep/high seas of the NE Atlantic. Biological Conservation **143**:1041-1056.

Howell, K. L., J. S. Davies, and B. E. Narayanaswamy. 2010. Identifying deep-sea megafaunal epibenthic assemblages for use in habitat mapping and marine protected area network design. Journal of the Marine Biological Association of the United Kingdom **90**:33-68.

Hyams-Kaphzan, O., H. Lubinevsky, O. Crouvi, Y. Harlavan, B. Herut, M. Kanari, M. Tom, and A. Almogi-Labin. 2018. Live and dead deep-sea benthic foraminiferal macrofauna of the Levantine basin (SE Mediterranean) and their ecological characteristics. Deep Sea Research Part I: Oceanographic Research Papers **136**:72-83.

Incarbona, A., B. Martrat, P. G. Mortyn, M. Sprovieri, P. Ziveri, A. Gogou, G. Jordà, E. Xoplaki, J. Luterbacher, and L. Langone. 2016. Mediterranean circulation perturbations over the last five centuries: Relevance to past Eastern Mediterranean Transient-type events. Scientific reports **6**:1-10.

IOLR. 2016. מאפיינים פיסיקליים של עמודת המים. IOLR.

IUCN. 2019. Thematic Report – Conservation Overview of Mediterranean Deep-Sea Biodiversity: A Strategic Assessment. IUCN Gland, Switzerland and Malaga, Spain.

Kanari, M., G. Tibor, J. Hall, T. Ketter, G. Lang, and U. Schattner. 2020. Sediment transport mechanisms revealed by quantitative analyses of seafloor morphology. New evidence from multibeam bathymetry of the Israel Exclusive Economic Zone. Journal of Marine and Petroleum Geology.

Katz, T., Y. Weinstein, R. Alkalay, E. Biton, Y. Toledo, A. Lazar, O. Zlatkin, R. Soffer, E. Rahav, and G. Sisma-Ventura. 2020. The first deep-sea mooring station in the eastern Levantine basin (DeepLev), outline and insights into regional sedimentological processes. Deep Sea Research Part II: Topical Studies in Oceanography **171**:104663.

Kreft, H., and W. Jetz. 2010. A framework for delineating biogeographical regions based on species distributions. Journal of Biogeography **37**:2029-2053.

Last, P. R., V. D. Lyne, A. Williams, C. R. Davies, A. J. Butler, and G. K. Yearsley. 2010. A hierarchical framework for classifying seabed biodiversity with application to planning and managing Australia's marine biological resources. Biological Conservation **143**:1675-1686.

Levin, N., T. Mazor, E. Brokovich, P.-E. Jablon, and S. Kark. 2015. Sensitivity analysis of conservation targets in systematic conservation planning. Ecological Applications **25**:1997-2010.

Liaw, A., and M. Wiener. 2002. Classification and regression by randomForest. R news **2**:18-22.

Madden, C. J., and D. H. Grossman. 2004. A framework for a coastal/marine ecological classification standard. NatureServe, Arlington, VA. Prepared for the National Oceanic and Atmospheric Administration, Under Contract EA-133C-03-SE-0275.

Magneville, C., N. Loiseau, C. Albouy, N. Casajus, T. Claverie, A. Escalas, F. Leprieur, E. Maire, D. Mouillot, and S. Villéger. 2021. mFD: a computation of functional spaces and functional indices. R package version 1.0. 0.

Makovsky, Y., O. Bialik, A. Neuman, and M. Rubin-Blum. 2020. Rare habitats at the seafloor of Palmahim disturbance – Mapping and characterization for the purpose of conservation. University of Haifa, IOLR,.

Marbà, N., G. Jordà, S. Agusti, C. Girard, and C. M. Duarte. 2015. Footprints of climate change on Mediterranean Sea biota. Frontiers in Marine Science **2**:56.

Marras, S., A. Cucco, F. Antognarelli, E. Azzurro, M. Milazzo, M. Bariche, M. Butenschön, S. Kay, M. Di Bitetto, and G. Quattrocchi. 2015. Predicting future thermal habitat suitability of competing native and invasive fish species: from metabolic scope to oceanographic modelling. Conservation physiology **3**:cou059.

Mouillot, D., S. Villéger, V. Parravicini, M. Kulbicki, J. E. Arias-González, M. Bender, P. Chabanet, S. R. Floeter, A. Friedlander, and L. Vigliola. 2014. Functional over-redundancy and high functional vulnerability in global fish faunas on tropical reefs. Proceedings of the National Academy of Sciences **111**:13757-13762.

Nykjaer, L. 2009. Mediterranean Sea surface warming 1985–2006. Climate Research **39**:11-17.

Ozer, T., I. Gertman, N. Kress, J. Silverman, and B. Herut. 2017. Interannual thermohaline (1979–2014) and nutrient (2002–2014) dynamics in the Levantine surface and intermediate water masses, SE Mediterranean Sea. Global and Planetary Change **151**:60-67.

Phillips, S. J. 2021. maxnet: Fitting 'Maxent' Species Distribution Models with 'glmnet'. R package version 0.1.4.

Phillips, S. J., R. P. Anderson, and R. E. Schapire. 2006. Maximum entropy modeling of species geographic distributions. Ecological modelling **190**:231-259.

Poiani, K. A., B. D. Richter, M. G. Anderson, and H. E. Richter. 2000. Biodiversity conservation at multiple scales: functional sites, landscapes, and networks. BioScience **50**:133-146.

Rengstorf, A. M., A. Grehan, C. Yesson, and C. Brown. 2012. Towards high-resolution habitat suitability modeling of vulnerable marine ecosystems in the deep-sea: resolving terrain attribute dependencies. Marine Geodesy **35**:343-361.

Rilov, G. 2016. Multi-species collapses at the warm edge of a warming sea. Scientific reports **6**:1-14.

Rilov, G., and B. Galil. 2009. Marine bioinvasions in the Mediterranean Sea–history, distribution and ecology. Pages 549-575 Biological invasions in marine ecosystems. Springer.

Rivetti, I., S. Fraschetti, P. Lionello, E. Zambianchi, and F. Boero. 2014. Global warming and mass mortalities of benthic invertebrates in the Mediterranean Sea. PLOS ONE **9**:e115655.

Roff, J. C., and M. E. Taylor. 2000. National frameworks for marine conservation—a hierarchical geophysical approach. Aquatic Conservation: Marine and Freshwater Ecosystems **10**:209-223.

Roff, J. C., M. E. Taylor, and J. Laughren. 2003. Geophysical approaches to the classification, delineation and monitoring of marine habitats and their communities. Aquatic Conservation: Marine and Freshwater Ecosystems **13**:77-90.

Rubin-Blum, M., G. Sisma-Ventura, Y. Yudkovski, N. Belkin, M. Kanari, B. Herut, and E. Rahav. 2022. Diversity, activity, and abundance of benthic microbes in the Southeastern Mediterranean Sea. FEMS Microbiology Ecology **98**.

Shapiro Goldberg, D., I. Van Rijn, M. Kiflawi, and J. Belmaker. 2019. Decreases in length at maturation of Mediterranean fishes associated with higher sea temperatures. ICES Journal of Marine Science **76**:946-959.

Simpson, E. H. 1949. Measurement of diversity. Nature **163**:688-688.

Simpson, G. G. 1960. Notes on the measurement of faunal resemblance. American Journal of Science **258**:300-311.

Somot, S., F. Sevault, M. Déqué, and M. Crépon. 2008. 21st century climate change scenario for the Mediterranean using a coupled atmosphere–ocean regional climate model. Global and Planetary Change **63**:112-126.

Spanier, E., and B. S. Galil. 1991. Lessepsian migration: a continuous biogeographical process. Endeavour **15**:102-106.

Therneau, T., and B. Atkinson. 2022. rpart: Recursive Partitioning and Regression Trees. R package version 4.1.16.

van Rijn, I., Y. Buba, J. DeLong, M. Kiflawi, and J. Belmaker. 2017. Large but uneven reduction in fish size across species in relation to changing sea temperatures. Global Change Biology **23**:3667-3674.

Williams, A., N. J. Bax, R. J. Kloser, F. Althaus, B. Barker, and G. Keith. 2009. Australia's deep-water reserve network: implications of false homogeneity for classifying abiotic surrogates of biodiversity. ICES Journal of Marine Science **66**:214-224.

Yeruham, E., M. Shpigel, A. Abelson, and G. Rilov. 2020. Ocean warming and tropical invaders erode the performance of a key herbivore. Ecology **101**:e02925.

Zurell, D. 2020. mecofun: useful functions for macroecology and species distribution modelling version 0.0.0.9.

Annexes

Annex 1

This Annex provides detailed description of hierarchical levels used in representative benthic ecological units classification

Province

The Levantine basin is the eastern-most part of the Mediterranean Sea and covers about 320000 km^2. The basin is oligotrophic and generally warmer and saltier than the western Mediterranean. The area is strongly affected by climate change. The average sea surface temperature in the Levant region has increased by about 1.1 degrees in the past century, and it is predicted to increase by a further 2.3–2.9°C by the end of this century (Somot et al. 2008, Nykjaer 2009, Rilov 2016, Ozer et al.

2017). The marine biota in the Mediterranean Sea is reacting to this by changes in life cycles, demography and distribution (Ben Rais Lasram et al. 2010, Rivetti et al. 2014, Marbà et al. 2015, Rilov 2016, van Rijn et al. 2017, Shapiro Goldberg et al. 2019, Yeruham et al. 2020). In addition to its response to elevated water temperatures, the Levant biota is rapidly changing due to the influx of hundreds of invasive species from the Red Sea through the Suez Canal (Bianchi 2007, Rilov and Galil 2009, Marras et al. 2015). The opening of the Suez Canal initiated an event of joining of two biogeographical provinces. For over 120 years, Red Sea species, migrating through the canal, have been colonizing the Mediterranean (Spanier and Galil 1991). Until now, more than 650 alien species were recorded, about 30% most are mollusks, crustaceans, fish and macrophytes. It has been postulated that these mostly thermophilic invaders may be able to better resist the rising temperatures and hence be less affected, or even facilitated, by warming waters (Gamliel et al. 2020).

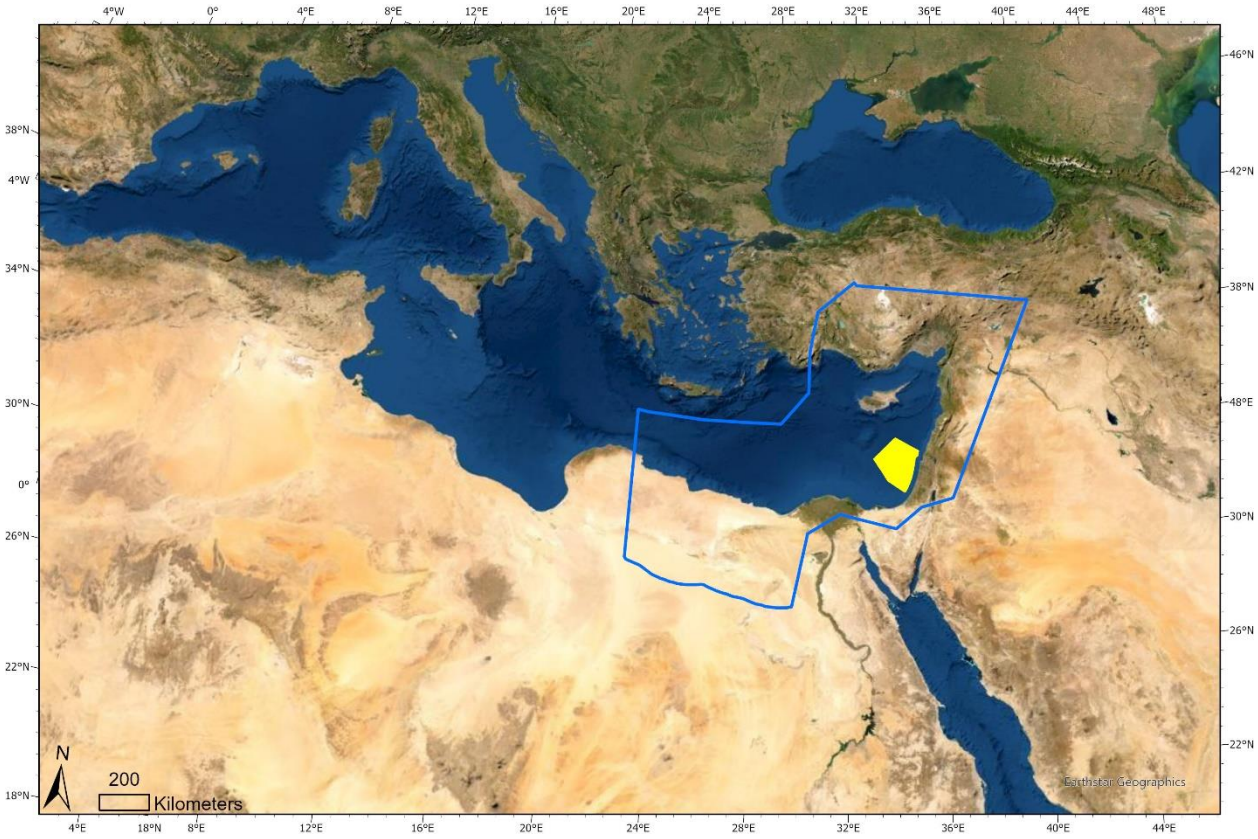

Figure A1. The Levantine basin of the Mediterranean Sea (blue line) and Israeli EEZ (yellow polygon). The Levantine basin is the province of the EEZ based on common biogeographic definition.

Bathomes

It is widely accepted that the deep-sea fauna undergo a non-repeating sequential change with depth and that most species have predictable and restricted depth ranges (Howell 2010). However, it is not the depth per-se that influences biological communities, but rather the abiotic parameters that change along depths gradients. These are more easily measured and widely accepted surrogate for the combined influence of these environmental parameters on benthic biological communities (Howell 2010).

This pattern is reflected in the results and conclusions of recent studies on water masses and transport dynamic along the Israeli coast (Katz et al. 2020, Guy-Haim et al. 2022).

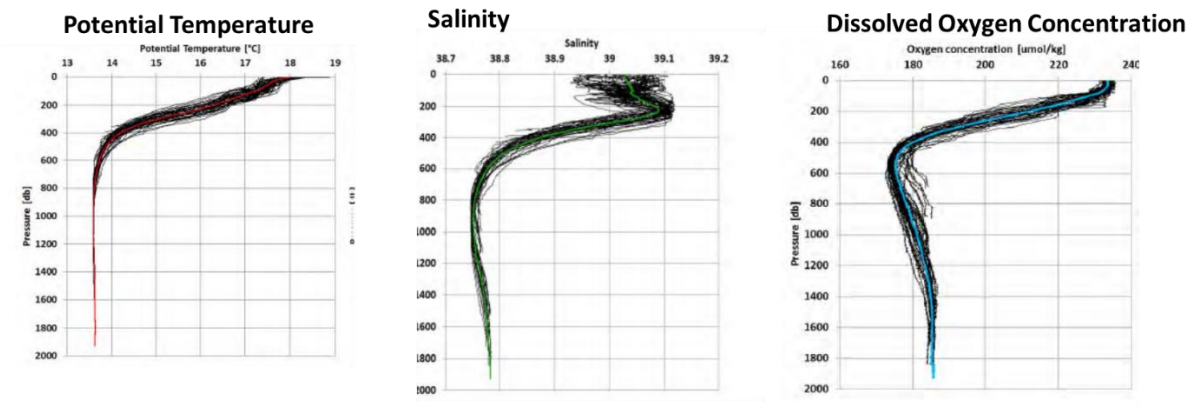

Figure A2. Vertical transects of temperature, salinity and dissolved oxygen in the Israeli EEZ (IOLR 2016). Below 600 m depth, changes in these parameters are minor compared with shallower depth.

Therefore, we adopted the bathymetric depth ranges that are commonly used for the Israeli EEZ of -200 m – (-)1000 m and below -1000 m, and added a subdivision of the slope in -600 m to reflect the water masses classification of IOLR (2016).

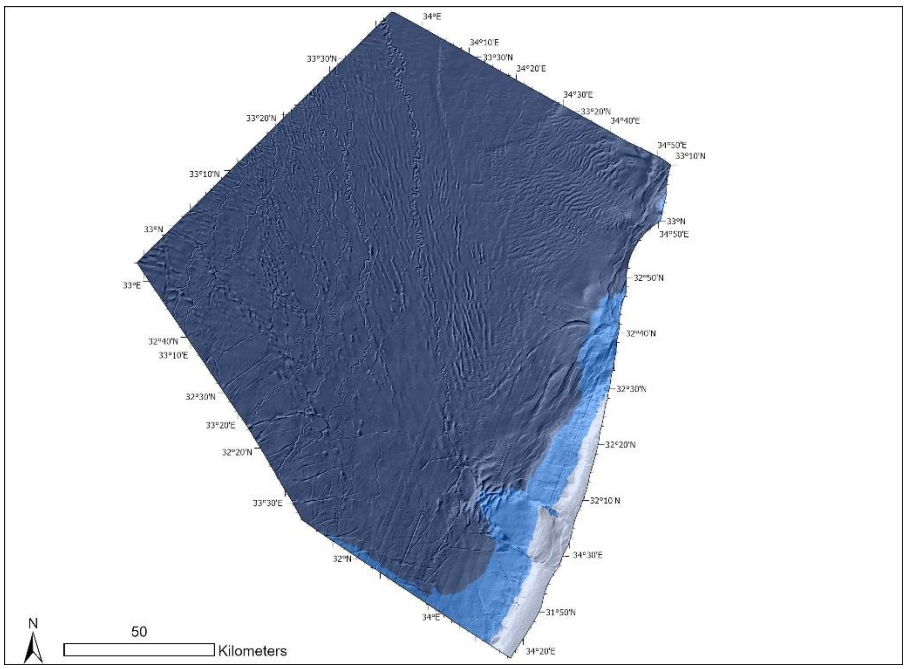

Figure A3. Bathomes in the EEZ. Upper slope: -200 m – (-)600 m (gray), Lower slope: -600 m – (-)1000 m (light blue), and Deep bathyal plateau: <-1000 m (dark blue).

Geomorphology

Integrating geomorphology is at the base of the ecotipological approach for the classification of benthic marine ecosystems (Bianchi and Zurlini 1984). The use of seabed features and geomorphology in classifying and mapping the marine environment is widespread (Greene et al. 1999, Allee et al. 2000, Connor et al. 2006, Harris 2007) and geomorphic features are widely considered as individual habitats or habitats type (Ceccarelli et al. 2021). As highlighted by Williams et al. (2009), these features are biologically meaningful in terms of MPA network design and has been largely driven by the political imperative to develop MPA networks over relatively short timescales and for vast areas of the deep-sea.

Based on our accumulating observations and experience, and in line with accepted global practices (e.g., Harris and Baker 2011), we assume that the deep-sea habitats in the Israeli EEZ are controlled, at least to a great degree, by the seafloor geomorphology. Here 'geomorphology' is taken at its broad context as the accumulation of geological, geochemical, morphological and oceanographic factors that shape the seafloor environment. Several major factors affecting the Israeli EEZ include:

1. The Israeli EEZ seafloor forms the eastern part of the outlet cone, and litoral cell, of the Nile river, being the major source in the region. The variability of the seafloor domains in the region is primarily controlled by the by-pass transport of sediments and nutrients from and along the continental margin vs. their direct transport from the Nile outlet. In this context we include the activity of current regimes at different time scales, and down-slope gravity flows, producing a variety of seafloor morphologies and compositional variability.
2. Deformation associated with movement of the Messinian salt layer and overlaying sediments, producing pronounced morphological features and focusing sub-seafloor and oceanographic flows.
3. Current and past seepage of natural gasses, primarily methane, in the sub-surface and through the seafloor, and formation of associated pockmarks, bioturbation and carbonate rocks at the seafloor; as well as their potential contribution to the marine environment at large. In this context we believe that the natural gas hydrates stability, estimated to intersect the seafloor of the Israeli EEZ at the water depth of ~1200-1300 m, affects the deeper regions of the basin.

The studies of Gvirtzman et al. (2015) and Kanari et al. (2020) are describing the geomorphology along the Israeli Mediterranean coast (Figure 6). In this project, we adopted the geomorphic features classification described in these studies, in addition to the Hydrate stability boundary to define geomorphic domains in the EEZ**:**

Open slope/ canyons- The Israeli EEZ stretches across the southeastern Mediterranean continental shelf (average slope ~1-2 degrees) and slope (average slope of ~6 degrees) and into the southeastern part of the Levant basin (average slope ~1-2 degrees). The general shape of the continental slope changes from south to north from being *generally simple and relatively smooth and rounded* (=Open) south of Hadera, to *steep and cut by sharp canyons* to the north of Dor. The latter domain is in territorial waters, so in this project we did not define it as a separate geomorphological domain.

Submarine mass transport- is a general name given to features that are associated with displacement of sediments. This includes slides, **slumps** (sort of avalanches of sediments), debris flows, etc. In the context of the Israeli offshore geomorphology related to this project they are taking together to include a range of instantaneous failure and collapse features, leaving sharp scars on the open slope and fans of sediment debris lobes below; or mobilization features, like Palmahim Disturbance. Strictly speaking also the canyons and channels are mass transport features, but we discuss them separately. These features are scattered along the continental slope, as discussed in Katz et al. (2020) and Gadol et al. (2020).

Folds- Much of the seafloor of the Israeli EEZ overlies a layer of salt (the Messinian salt). The salt is plastic, like slowly moving honey, and it moves with the overlaying sediments northwards away from the loads of sediments accumulation in the Nile delta from one side, and westwards away from the

accumulating continental margin of Israel. This movement is semi continuous for at least the last 2 millions of years. As the sediments layer is moving with the salt it deforms, slightly folding to form fold ridges perpendicular to the direction of motion (like curtains when you push them aside).

Faults- In addition, the sediment layer tears and breaks along fault lines, forming steps, scars and slits of various sizes at the seafloor.

Sediment waves- are dune-like ridges that are formed by strong currents above the seafloor. At a first glance the bathymetric expressions of folds and sediment waves seem very similar, and sometimes people argue what these ridges are. The distinction is significant, as folds represent internal deformation of the sediments while sediments waves indicate the presence of strong seafloor currents (now or in the recent geological past)

Deep-Water Channel- levee systems- In the basin seafloor we find meandering channels (also called "**turbidity channels**"), sort of river like features (similar to the Jordan river south of the Kinneret, just much bigger), that are hundreds of meters wide and up to ~40 m deep. These channels run from the foots of the Nile Delta, hundreds of kilometers northwards to the Cypriot deeps. They are formed by fast and slick mud flows, gathering energy as the run down the slope. We do not know if any of these channels are active nowadays, and they are braded with older, now abandoned and buried, **paleo-channels**. The eastern-most of these channels was named by Gvirtzman et al. (2015) Levant Channel. At least this channel has probably not conducted such mud flows for thousands of years. The banks (levees) of these channels are elevated, due to over-spill of mud running inside the channels. In some places the mud escaped from the channels, flooding the near-by plains and leaving their thin layers of sediments (flood-plain or overbank deposits). Sometimes such channels form little deltas, or fan lobes. Together, this set of features (and additional related features) are named deep-water channel-levee systems. The Levant channel is conceptually not different from the other channels, it is just the closest to our shoreline and Gvirtzman decided to name it.

In addition to the above, we used **Hydrate stability boundary** to define the geomorphic domains- Natural hydrates are ices forming within the seafloor or sub-seafloor sediment at ambient temperature (possibly much above zero Celsius) when pressure is high enough. Their formation is associated with the presence of gas components, most commonly methane. Their formation locks the methane into the ice and stabilizes the seafloor/soil, while their melting allows the release of methane and destabilizes (as is currently happening in permafrost regions). Our modeling indicated that at present conditions the hydrate stability is reached in the Levant as a water depth of ~1250 m. Allowing slight variability of these conditions we say that hydrate stability is reached here between 1200-1300 m water depth. Thus hydrates may be present at or below the seafloor at greater water depths.

Biotopes

The use of substrate in habitat classification systems is universal and its validity as a fine scale surrogate for deep-sea faunal variation is well established (Howell 2010). There are well recognized and accepted definitions of substratum type, however, the categories often require simplifying into easily interpretable units that remain at least broadly biologically meaningful (Harris 2020). Common substrate types that are used in classification systems are: rock, sand, muddy sand, and mud (e.g., Davies and Moss 1998, Davies et al. 2004, Last et al. 2010).

Sediments grain size in the Israeli EEZ are detailed in Elyashiv and Cruvi Elyashiv and Kruvi (2016) GSI and IOLR report. This report was based on a single expedition in 2013 where 104 sediment samples were taken from 52 stations in the Israeli EEZ. It was found that most (45-85%) of the

grains in the sediment are clay (size-based classification), 25-55% is silt and the sand fraction is not more than 12%. Grain size generally decreases with depth and distance from the coastline (clay increases and silt decreases). This corresponds with the primary siliciclastic (grains with a prominent silicate composition) character of the sediments, with their primary source being the Nile River outpour. From there the sediments are supplied directly into the deep-sea fan, constituting the major part of the deep basin in the area, and through a by-pass flow along and off of the continental margin of Israel. Altogether, the plan area is characterized with a low diversity of sediments, resulting from the long supply distance of the siliciclastic sediments. Moreover, the carbonate detritus in the sediment weaken the correlation of grain size with the depth and distance from the coast, as this detritus come mostly from pelagic and benthic biogenic origin. However, notable in this respect is the significant contribution of carbonate to the sand fraction, and particularly in the deeper parts of the basin, indicating the biogenic source of most of the sand-size grains.

The preliminary mapping of the sediments composition carried by (Elyashiv and Kruvi 2016) used depth weighted interpolation (DWI), which tend to highlight the effects of outlier observations over spatial trends. To extract the spatial trends of the data, attenuating outliers, we re-modelled the sediments distribution in the EEZ with a process constrained regression approach (see methods).

Regression equations used in sediment distribution modelling

Water depth > 600m

d10= -0.66213*(log(water depth)) + 3.454657

d50= 0.137206*(SILT) + 1.05266

d90= 4.972349557*(SAND) + 18.74643526

CLAY= 100 - SILT - Sand

SILT= -16.1917*(log(water depth)) - 1.7805*(Longitude [DD]) + 142.3108

SAND=10^(1.9471*(log(water depth))^2 - 9.7842*(log(water depth))+ 11.816)

TOC= -1.31793*(log(water depth)) + 4.96597

Water depth < 600m

d10= 0.001114*water depth + 2.142989

d50= 464.2*(log(water depth)) ^ -5.051

d90= 524.97*(log(water depth)) ^ -2.948

CLAY=34.25145*(log(water depth)) - 45.8858

SILT= 57.51493*(log(water depth)) - 56.0912

SAND=1663.9*(log(water depth)) ^ -7.788

TOC=0.804675*(log(water depth)) - 0.84855

Biological assemblages

Biological facies are the fundamental units for the management of biodiversity, being firmly nested within all levels above and acting as surrogates for all levels below. Facies are characterized by groups or particular species of macro-biotic groups, yet, mobile taxa such as fish are likely to be less informative discriminators of facies than sessile animals (Last et al. 2010).

Micro-communities are defined as small-scale assemblages of often highly specialized species that depend on other member species or groups of species within a 'host' facies. In general, adequate protection of facies-level units will ensure conservation of their associated micro-communities. Typical micro-communities include infauna of muddy sediments, and epifauna in chemosynthetic assemblages (Last et al. 2010). We relate to biological facies and micro-communities as biological assemblages.

The dataset (see Table 1) – after pruning vertebrates, pelagic taxa, samples in unusable taxonomic scale or likely erroneous samples – consisted of:

332 taxa (110 benthic, 6 bentho-pelagic, 167 infauna, 49 no habitat type data available).

4009 observations (1439 benthic, 31 benthopelagic, 2022 infauna, 517 no habitat type data available).

Preliminary analyses using the same methodology were performed on taxa separated by habitat type – however, the results of the classification were strongly congruent between different datasets, and so the report includes only analyses performed on the full dataset, as it has the highest sample size and provides the best predictive capability.

Here are further explanations on the selected methods and functions that were used:

- Data were projected onto a grid consisting of 0.1*0.1 decimal degree cells – Cell size was chosen to give a wider spatial coverage (since sampling was sporadic with multiple unsampled areas) without losing too much spatial resolution in sampling, while assuming that the cell size is small enough to likely capture contiguous assemblages.
- Sampling data in the EEZ vary in sampling effort, methods, periods, and taxonomic analyses. Therefore, samples are likely to vary in overall alpha diversity. Therefore, the clustering methodology followed (Castro-Insua et al. 2018) - Dissimilarity between cells was calculated using the Simpson dissimilarity index (Simpson 1960), which was deemed the most fitting for this dataset as it is independent of differences in alpha diversity (species richness) between cells (Kreft and Jetz 2010, Baselga and Leprieur 2015). The Simpson dissimilarity index is more appropriate than indices which also reflect differences in species richness (e.g. Jaccard dissimilarity) or abundance (e.g. Bray-Curtis dissimilarity).
- Hierarchical clustering was performed on the dissimilarity matrix using the Ward clustering to minimizes dissimilarities within clusters and maximizes dissimilarities between clusters, and thus generated a dendrogram representing similarity between cells and groups of cells.
- To compare patterns of diversity between cells and clusters, Alpha diversity for each cell and cluster was calculated with the Simpson index (Simpson 1949) using the *diversity* function in the 'vegan' package. Beta diversity was then calculated between clusters using Sorensen dissimilarity, partitioned into turnover and nestedness components, with the *beta.pair* function. Then, functional diversity for each cluster was calculated using the 'mFD' package v1.0.0 (Magneville et al. 2021)
- A GDM was constructed using the *gdm* function in the 'gdm' package v1.5.0-3 (Fitzpatrick et al. 2022). Biological distances between faunal communities were measured using Simpson dissimilarity, see above)

- To build the GDM model, abiotic parameters measured in the 50 m above seafloor were considered (see Table 2) and the following bathymetric features were considered (all calculated on a 2km grid from raw 25m resolution bathymetry data, to match the final cell size used for delimiting ecological units for the MARXAN model):

1. Mean aspect
2. Mean bpi (250 m window)
3. Mean bpi (75 m window)
4. Mean depth
5. Maximum slope

Additionally, Euclidean distances at a 2km resolution were calculated from the nearest following Kanari et al. (2020) bathymetric features:

6. Faults
7. Folds
8. Slumps
9. Turbidity channels
10. Overbank deposits
11. Paleo channels
12. Fan lobes

Features 8 through 12 being components of the Nile fan deep-water channel-lobe systems.

And finally, the concentration of the following sediment elements was calculated:

13. Sand
14. Silt
15. Clay
16. Organic matter (d50)

- In the GDM the response values were Simpson dissimilarity measures between cells at a 2 km resolution – the calculation of assemblages per cell was similar to that described above for the 0.1 degree cells, but a 2 km resolution was chosen for GDM analyses to better capture variation in the environmental predictors.
- Uncertainty around the I-splines depicting the functional responses of compositional dissimilarity to each environmental predictor was plotted using the *plotUncertainty* function from the 'gdm' package,
- Spatial predictions for compositional dissimilarity were then generated for each environmental predictor based on the final GDM model, and the predictions were projected onto three-dimensional ordinated space using a PCA. The PC values were then scaled to RGB color channels to generate a map where dissimilarity in colors represents predicted biological dissimilarity.
- The additional SIMPER (similarity percentage; (Clarke 1993) for the final biological assemblage polygons, were run using the *simper* function in the 'vegan' package. SIMPER performs decomposition of Bray-Curtis dissimilarity to calculate the contribution of each taxon in a community matrix to dissimilarity – since abundance data are needed for this analysis, pseudo-abundance was calculated for each biological assemblage as the sum of unique observations per taxon – this reflects taxa that are especially common since they were observed multiple times in independent samples. Taxa that contribute at least to 70% of the difference between each pair of biological assemblages were identified as the most important to differentiation between assemblages.

- For each biological assemblage, the following description is included:

❖ wide-spread taxa - found in >50% cells comprising the assemblage
❖ unique taxa - only found in that assemblage
❖ potential indicative taxa - both wide-spread and unique
❖ represented functional entities
❖ over-represented functional entities - high functional over-redundancy

The following are further graphical results for biological assemblage characterization:

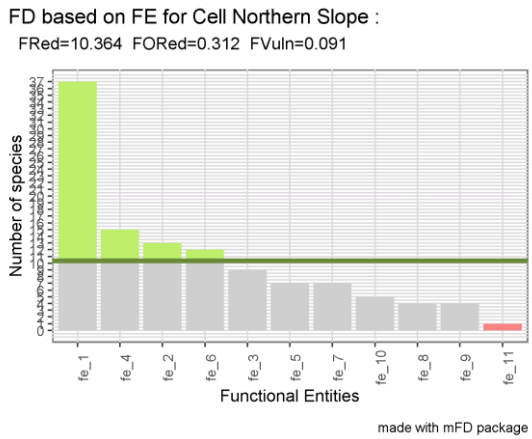

Figure A4. Functional diversity of the Northern Slope biological assemblage. FRed: Functional redundancy (number of taxa per functional entity), denoted by horizontal green line. FORed: Functional over redundancy (the proportion of taxa in functional entities above the mean level of functional redundancy), denoted by green shaded bars above the horizontal line. FVuln: Functional vulnerability (the proportion of functional entities with only a single taxon), denoted by red bars.

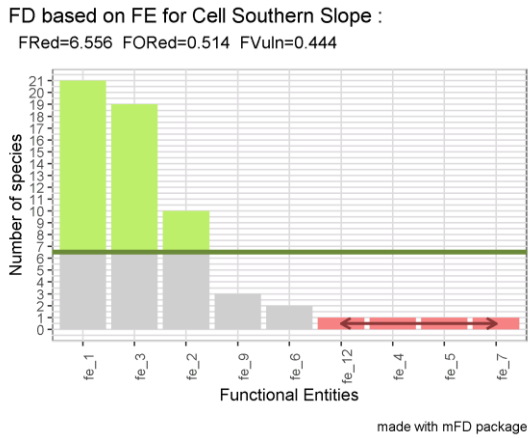

Figure A5. Functional diversity of the Southern Slope biological assemblage. FRed: Functional redundancy (number of taxa per functional entity), denoted by horizontal green line. FORed: Functional over-redundancy (the proportion of taxa in functional entities above the mean level of functional redundancy), denoted by green shaded bars above the horizontal line. FVuln: Functional vulnerability (the proportion of functional entities with only a single taxon), denoted by red bars.

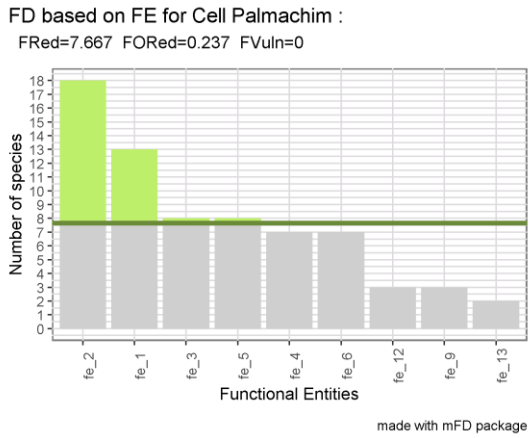

Figure A6. Functional diversity of the Palmahim biological assemblage. FRed: Functional redundancy (number of taxa per functional entity), denoted by horizontal green line. FORed: Functional over-redundancy (the proportion of taxa in functional entities above the mean level of functional redundancy), denoted by green shaded bars above the horizontal line. FVuln: Functional vulnerability (the proportion of functional entities with only a single taxon), denoted by red bars.

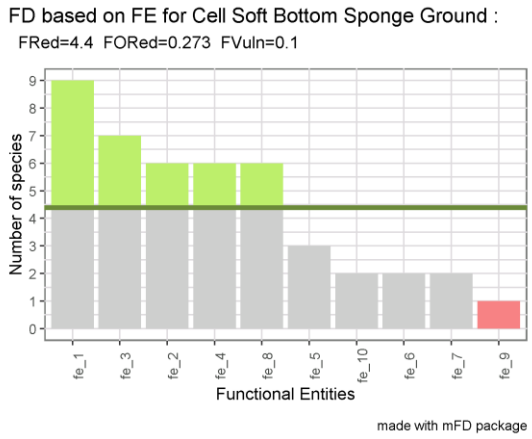

Figure A7. Functional diversity of the Soft Bottom Sponge Ground biological assemblage. FRed: Functional redundancy (number of taxa per functional entity), denoted by horizontal green line. FORed: Functional over-redundancy (the proportion of taxa in functional entities above the mean level of functional redundancy), denoted by green shaded bars above the horizontal line. FVuln: Functional vulnerability (the proportion of functional entities with only a single taxon), denoted by red bars.

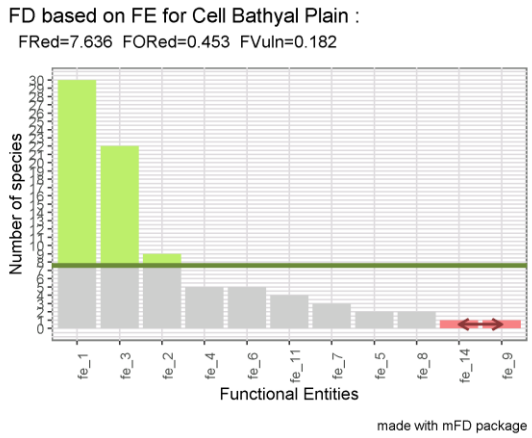

Figure A8. Functional diversity of the Bathyal Plain biological assemblage. FRed: Functional redundancy (number of taxa per functional entity), denoted by horizontal green line. FORed: Functional over-redundancy (the proportion of taxa in functional entities above the mean level of functional redundancy), denoted by green shaded bars above the horizontal line. FVuln: Functional vulnerability (the proportion of functional entities with only a single taxon), denoted by red bars.

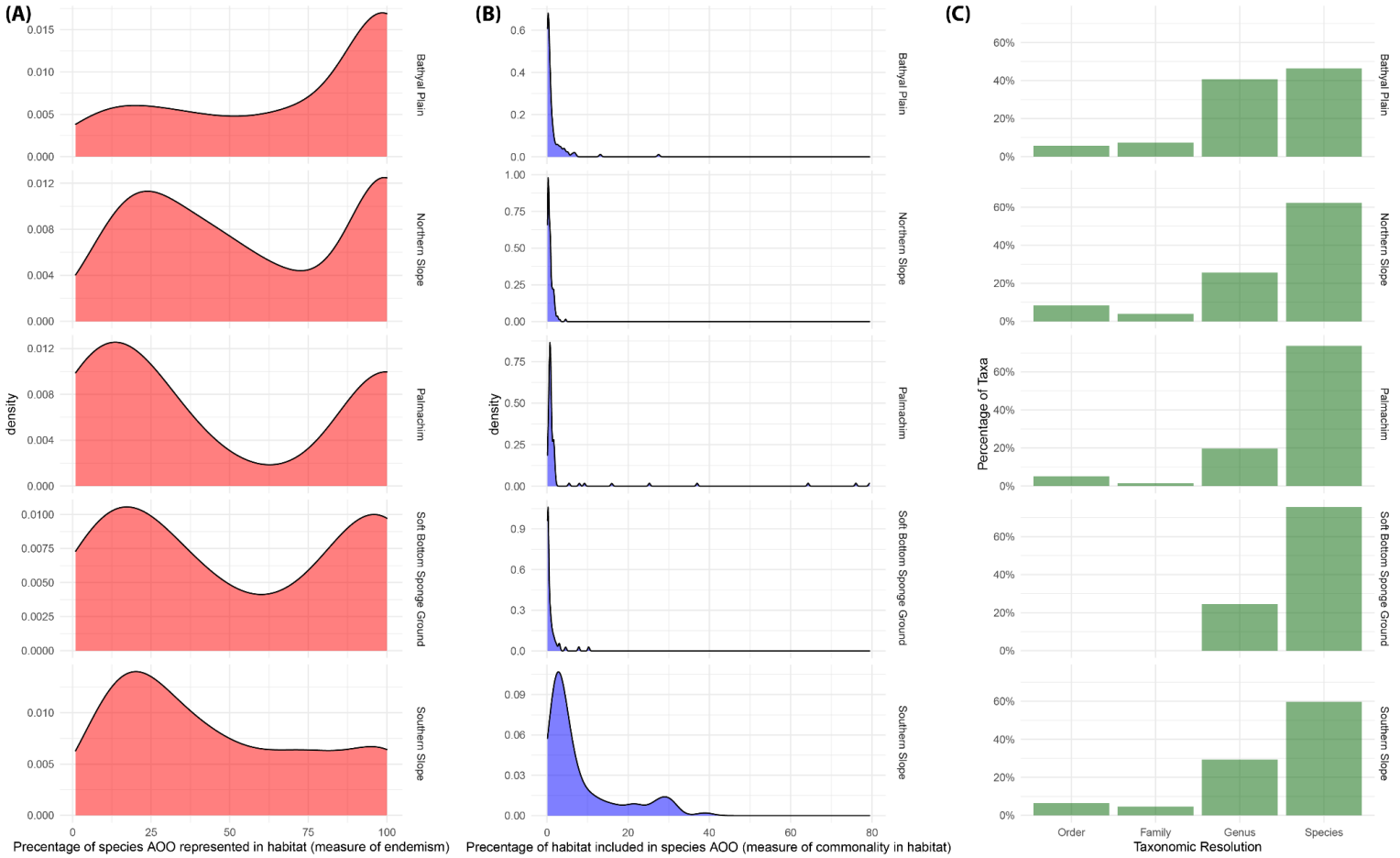

Figure A9. (A) Distributions of percentage of taxon AOO represented in each assemblage (measure of endemism); (B) Distributions of percentage of habitat area occupied by taxon AOO in each assemblage (measure of endemism); (C) Percentage of taxa identified to order, family, genus, and species level in each assemblage. Y axis in panels A and B is the probability density function for the kernel density estimation of the distribution.

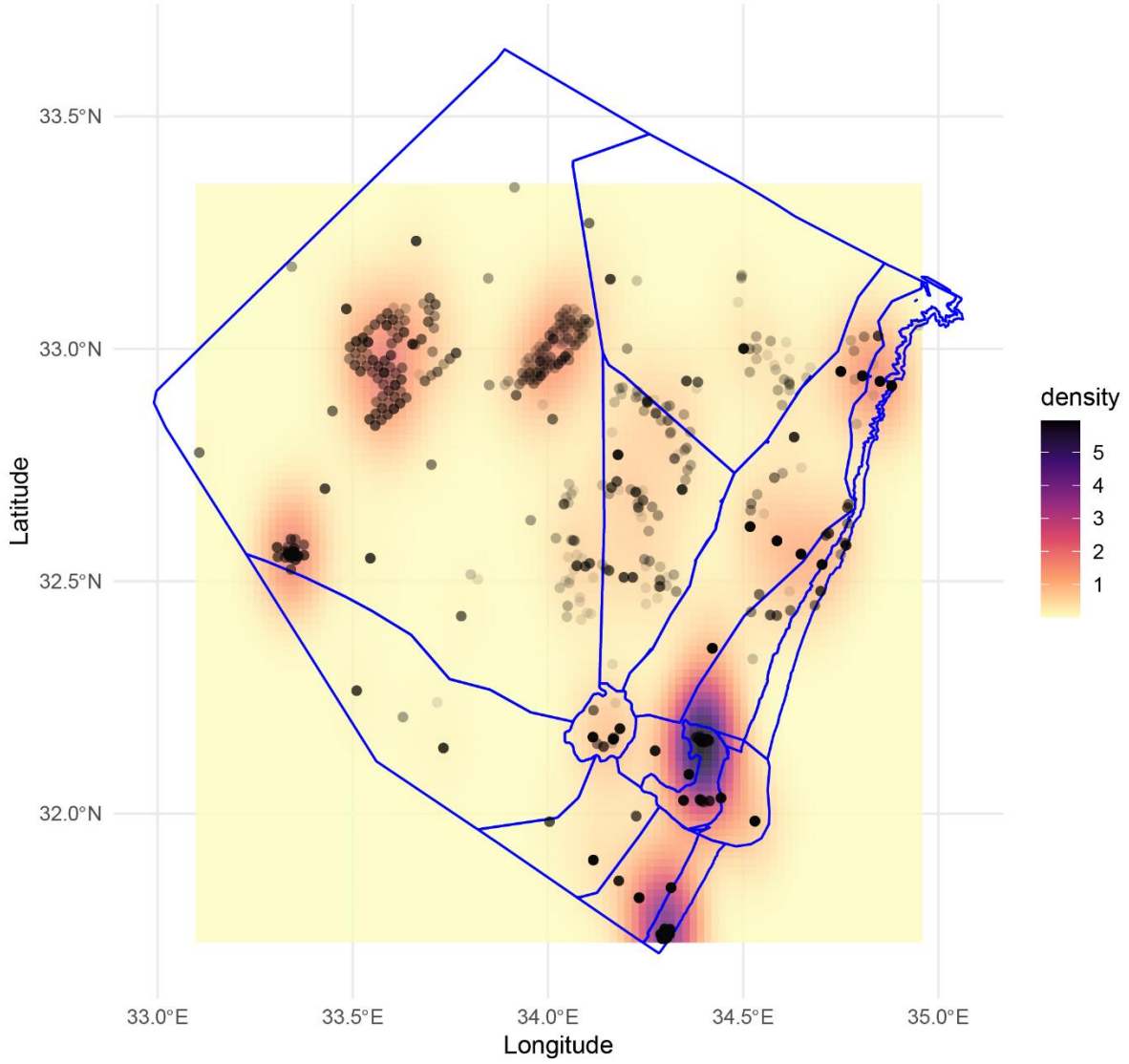

Figure A10. Map showing sampling density in the EEZ. Sampling localities are marked by black dots. Darker purple color represent higher density of sampling.

Foraminiferous

In addition to the biological assemblages we described using the database. We adopted the results of Hyams-Kaphzan et al. (2018) and (Almogi-Labin and Hyams-Kaphzan 2016) that classifies biological assemblages in the EEZ based on Foraminiferous species (dead and live assemblages).

They identified 104 live species and 208 dead species. Generally, species richness is low in the bathyal plain and community structure changes (correlated) with depth. At several sampling sites on the continental slope, they observed relatively high species richness. In addition, they point at unique epibenthic habitat in southern-west corner of the EEZ which is related to high carbonate concentrations caused by pteropods shells accumulation on this site. This pattern is also visualized by the carbonate concentration maps we used (see Methods section). The foraminifers aglutinante species (that usually inhabits bathyal domains in depths greater than -1200 m) are attached to the pteropods shells.

Foraminiferous species in the EEZ seems to be in high correlation with the biotopes that we classified. The habitats marked by Hyams-Kaphzan et al. (2018) and Almogi-Labin and Hyams-Kaphzan (2016) roughly align with the geomorphologic domains that were defined in this project. An exception is the unique epibenthic habitat that was found. Therefore, we included this area as additional biological assemblage in the EEZ, and used the results of the GDM to roughly mark its boundaries. Certainty score for this assemblage was defined as 1, only to distinguish it from areas where the biological assemblages are unknown, and from the other biological assemblages that had a minimum score of 2.6 (see Results).

Annex 2

This Annex provides further background and details on the methodology used for identifying unique benthic habiatats' distribution in the EEZ

Like species, some facies are spatially restricted or rare. These are often most vulnerable to impacts and may need to be given a high conservation priority. The identification of rare and threatened habitat at the facies-level is critical to the MPA selection process where protection of biodiversity is a major outcome. Therefore, specific taxa known as indicators of vulnerable marine ecosystem (VMEs) were separately analyzed for the next stage of mapping the distribution of unique habitats. By relating to unique benthic habitats, we achieve the purpose of Last's et al. (2010) Levels 6 and 7 as unique benthic habitats nest within our biological assemblage Level.

Species distribution models

The six different algorithms used to construct SDMs from the training set (presented in the Methods section but with further details on the function here):

1. Generalised Linear Models (GLMs) were fitted with a binomial family and logit link function, for both linear and quadratic terms of the predictor variables. Automated stepwise model selection based on AIC scores was then performed using the *step* function to remove non-informative predictor variables.

2. Generalised Additive Models (GAMs) were fitted with the *gam* function in the "gam" package v1.20.1 (Hastie 2022), using smooth splines with 4 degrees of freedom for each predictor variable.

3. Classification and regression trees (CARTs; Franklin 2010, Guisan et al. 2017) were fitted using the *rpart* function in the "rpart" package v4.1.16 (Therneau and Atkinson 2022). These grow a decision tree by repeatedly splitting the data to separate presences and pseudo-absences through searching along each environmental gradient for splitting rules. Internal cross-validation (xval) and minimum number of observations available to define a split (minsplit) were set at their default values of 10 and 20, respectively.

4. Random Forests (RFs; Hastie et al. 2009, Guisan et al. 2017) were fitted using the *randomForest* function in the "randomForest" package v4.7-1.1 (Liaw and Wiener 2002). These use a bagging (bootstrap aggregation) procedure to average outputs of multiple CARTs fitted to bootstrapped samples of the training set. The number of trees to grow (ntree) was set at 1000.

5. Boosted Regression Trees (BRTs) were fitted using the *gbm.step* function from the "dismo" package v1.3-5 (Hijmans et al. 2021), which implements the *gbm* function from the "gbm"

package v2.1.8 (Greenwell et al. 2020) while optimising the number of trees. These are similar to RFs in using a bagging procedure on multiple CARTs, but differ by iteratively building trees through sampling without replacement. The Bernoulli (=binomial) family was used, tree.complexity was set at 2, and bag.fraction and learning.rate were set at their default values of 0.75 and 0.001, respectively.

6. Maximum Entropy (MaxEnt; Phillips et al. 2006, Elith et al. 2011) models were fitted using the *maxent* function in the "maxnet" package v0.1.4 (Phillips 2021). These are presence-only models that minimise the relative entropy between the probability density of presences and the probability density of the environment, by contrasting occurrence data with background data (pseudo-absences) where presence is unknown.

The different measures for model performance (using the 30% test set) were calculated using the *evalSDM* function in the "mecofun" package v0.0.0.9 (Zurell 2020).

Annex 3

This Annex provides further background and details on the bathymetric data that were used

This work bases the determination of representative ecological units on a revised version of Kanari et al. (2020) bathymetric multibeam digital elevation model (DEM). The DEM, which covers the entire Israeli EEZ, was released for our use at a uniform grid resolution of 100 m. Correspondingly, we utilize the seafloor features, mapped by Kanari et al. (2020) and provided as shape files. However, the resolution of Kanari et al. (2020) bathymetric is not sufficient to reflect the scale of morphologic parameters, which we assume to control unique seafloor habitats. The mapping of these features is based on morphological attributes that were extracted from a higher, 25 m, resolution bathymetric DEM, which was created by combining the best resolution bathymetric datasets that are available for us across the EEZ. These include:

1. Seafloor picks of 3D seismic data, normally obtained at a 12.5 m grid resolution (after Gvirtzman et al., 2015).
2. Local multibeam grids, provided at 50 m resolution.

To fill in areas that are not covered by these datasets, Kanari et al. (2020) 100 m resolution DEM was used. All data were calibrated to Kanari et al. (2020) DEM, combined and re-grided to a uniform 25 m resolution. The bathymetric attributes where then measured from the high resolution data and mapped to the 2 km resolution of our modeling, providing the maximal or averaged values and the standard deviation or range in each 2 km grid cell. This allowed for habitat analyses at 2 km grid to be based on high resolution attributes.

Annex 4

Maps of abiotic variables used in GDM and SDM

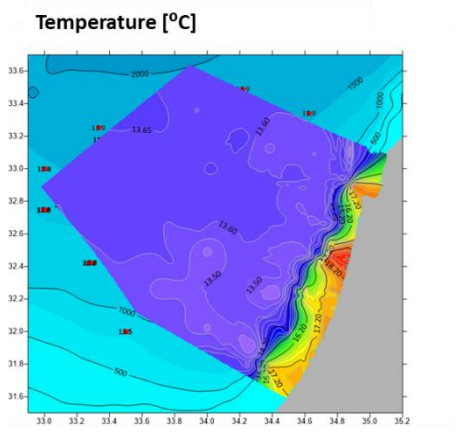

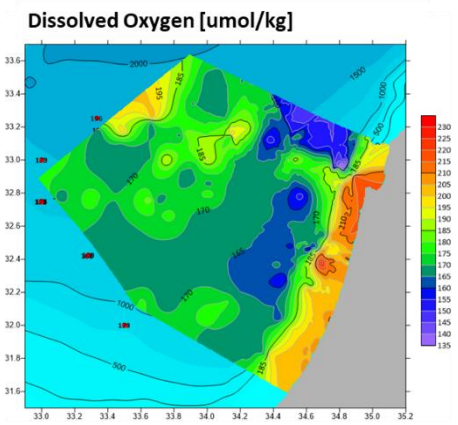

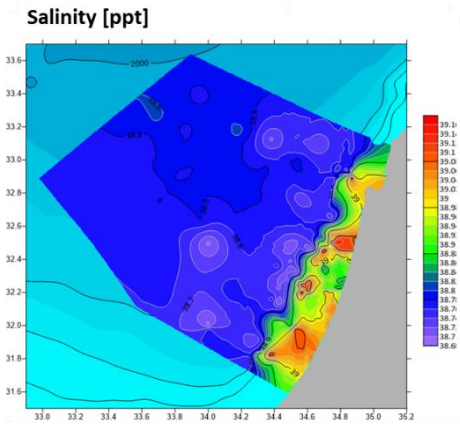

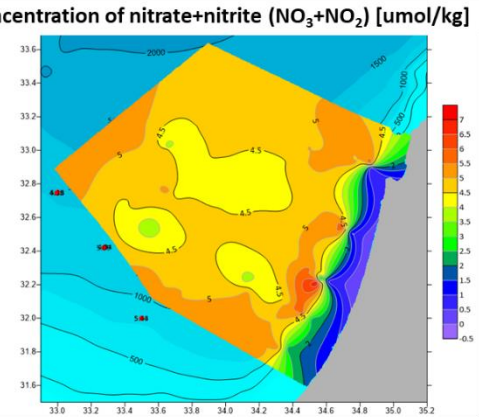

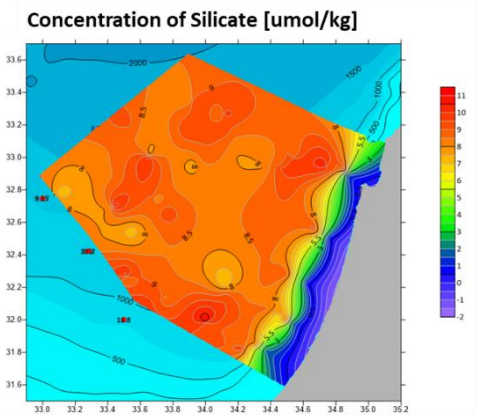

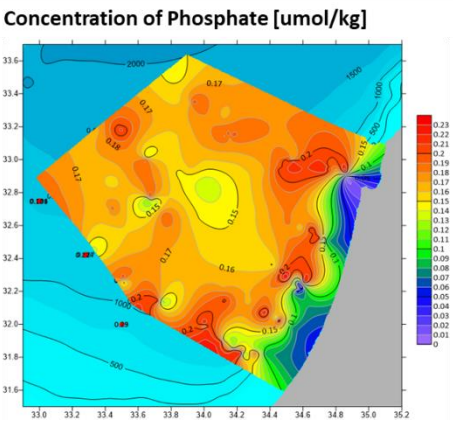

Annex 5

References used in data collection

1. Abelló, P., Ungaro, N., Politou, C.Y., Torres, P., Roman, E., Rinelli, P., Maiorano, P. and Norrito, G., 2001. Notes on the distribution and biology of the deep-sea crab Bathynectes maravigna (Brachyura: Portunidae) in the Mediterranean Sea. In *Advances in Decapod Crustacean Research* (pp. 187-192). Springer, Dordrecht.
2. Basso, D., Beccari, V., Almogi-Labin, A., Hyams-Kaphzan, O., Weissman, A., Makovsky, Y., Rüggeberg, A. and Spezzaferri, S., 2020. Macro-and micro-fauna from cold seeps in the Palmahim Disturbance (Israeli off-shore), with description of Waisiuconcha corsellii n. sp.(Bivalvia, Vesicomyidae). *Deep Sea Research Part II: Topical Studies in Oceanography*, *171*, p.104723.
3. Bozzano, A., Sardà, F. and Ríos, J., 2005. Vertical distribution and feeding patterns of the juvenile European hake, Merluccius merluccius in the NW Mediterranean. *Fisheries Research*, *73*(1-2), pp.29-36.
4. Ben-Eliahu, M.N. and Fiege, D., 1996. Serpulid tube-worms (Annelida: Polychaeta) of the Central and Eastern Mediterranean with particular attention to the Levant Basin. *Senckenbergiana maritima*, *28*(1), pp.1-51.
5. Bisby, F.A., Ruggiero, M.A., Wilson, K.L., Cachuela-Palacio, M., Kimani, S.W., Roskov, Y., Soulier-Perkins, A. and van Hertum, J., 2006. Species 2000 & ITIS Catalogue of Life: 2006.
6. Bogi, C. and Galil, B.S., 2013. New molluscan records from the eastern Mediterranean bathyal. *Marine Biodiversity Records*, *6*.
7. Follesa, M.C., Cannas, R., Gastoni, A., Cabiddu, S., Deiana, A.M. and Cau, A., 2008. Abnormal rostrum in Polycheles typhlops (Decapoda: Polychelidae) from the central western Mediterranean. *Journal of Crustacean Biology*, *28*(4), pp.731-734.
8. Carreton, M., Rotllant, G., Clavel-Henry, M., Bahamón, N., Sardà, F. and Company, J.B., 2021. Abundance and distribution of the deep-sea shrimp Aristeus antennatus larvae along the eastern Spanish Mediterranean coast (GSA 6). *Journal of Marine Systems*, *223*, p.103611.
9. Carrassón, M. and Matallanas, J., 2002. Diets of deep-sea macrourid fishes in the western Mediterranean. *Marine Ecology Progress Series*, *234*, pp.215-228.
10. Conlan, K.E., 2021. New genera for species of Jassa Leach (Crustacea: Amphipoda) and their relationship to a revised Ischyrocerini. *Zootaxa*, *4921*(1), pp.1-72.
11. Corbera, J., Segonzac, M. and Cunha, M.R., 2008. A new deep-sea genus of nannastacidae (Crustacea, cumacea) from the lucky strike hydrothermal vent field (Azores triple junction, mid-atlantic ridge). *Marine Biology Research*, *4*(3), pp.180-192.
12. Correa, M.L., Freiwald, A., Hall-Spencer, J. and Taviani, M., 2005. Distribution and habitats of Acesta excavata (Bivalvia: Limidae) with new data on its shell ultrastructure. In *Cold-water corals and ecosystems* (pp. 173-205). Springer, Berlin, Heidelberg.
13. Cunha, M.R., Matos, F.L., Génio, L., Hilário, A., Moura, C.J., Ravara, A. and Rodrigues, C.F., 2013. Are organic falls bridging reduced environments in the deep sea?-Results from colonization experiments in the Gulf of Cádiz. *PLoS One*, *8*(10), p.e76688.
14. Cusson, M., Archambault, P. and Aitken, A., 2007. Biodiversity of benthic assemblages on the Arctic continental shelf: historical data from Canada. *Marine ecology progress series*, *331*, pp.291-304.

15. d'Acoz, U., 1999. Inventaire et distribution des crustacés décapodes de l'Atlantique nord-oriental, de la Méditerranée et des eaux continentales adjacentes au nord de 25 N. *Collection des Patrimoines Naturels*, *40*, pp.1-383.
16. De Bruin, G.H.P., 1965. Penaeid prawns of Ceylon (Crustacea Decapoda, Penaeidae). *Zoologische Mededelingen*, *41*(4), pp.73-104.
17. Di Camillo, C., Bo, M., Puce, S., Tazioli, S., Froglia, C. and Bavestrello, G., 2008. The epibiontic assemblage of Geryon longipes (Crustacea: Decapoda: Geryonidae) from the Southern Adriatic Sea. *Italian Journal of Zoology*, *75*(1), pp.29-35.
18. Elder, Leanne E., and Brad A. Seibel. "The thermal stress response to diel vertical migration in the hyperiid amphipod Phronima sedentaria." *Comparative Biochemistry and Physiology Part A: Molecular & Integrative Physiology* 187 (2015): 20-26.
19. Fanelli, E., Colloca, F. and Ardizzone, G., 2007. Decapod crustacean assemblages off the West coast of central Italy (western Mediterranean). *Scientia Marina*, *71*(1), pp.19-28.
20. Galil, B., Diamant, A. and Horton, T., 2004. Ceratothoa steindachneri (Isopoda, Cymothoidae): An unusual record from the Mediterranean. *Crustaceana*, *77*(9), pp.1145-1148.
21. Galil, B.S., Danovaro, R., Rothman, S.B.S., Gevili, R. and Goren, M., 2019. Invasive biota in the deep-sea Mediterranean: an emerging issue in marine conservation and management. *Biological Invasions*, *21*(2), pp.281-288.
22. Gebruk, A.V., Krylova, E.M., Lein, A.Y., Vinogradov, G.M., Anderson, E., Pimenov, N.V., Cherkashev, G.A. and Crane, K., 2003. Methane seep community of the Håkon Mosby mud volcano (the Norwegian Sea): composition and trophic aspects. *Sarsia*, *88*(6), pp.394-403.
23. Giuste, F. and Sbrana, C., 2012. Lurifax vitreus Warén & Bouchet, 2001 (Gastropoda, Orbitestellidae), a new record for deep waters of the Tuscan Archipelago (Tyrrhenian Sea, Italy). *Biodiversity Journal*, *3*(1), pp.91-92.
24. Golani, D., 1986. On deep-water sharks caught off the Mediterranean coast of Israel. *Israel Journal of Zoology*, *34*(1-2), pp.23-31.
25. Goren, M., Danovaro, R., Rothman, S.B.S., Mienis, H.K. and Galil, B.S., 2020. Snapshot of the upper slope macro-and megafauna of the southeastern Mediterranean Sea: ecological diversity and protection. *Vie Milieu*, *69*, pp.233-248.
26. Goren, M. and Galil, B.S., 2015. A checklist of the deep-sea fishes of the Levant Sea, Mediterranean Sea. *Zootaxa*, *3994*(4), pp.507-530.
27. Goren, M., Mienis, H.K. and Galil, B.S., 2008. Not so poor—more deep-sea records from the Levant Sea, eastern Mediterranean. *Marine Biodiversity Records*, *1*.
28. Goren, M. and Galil, B.S., 1997. New records of deep-sea fishes from the Levant Basin and a note on the deep-sea fishes of the Mediterranean. *Israel Journal of Zoology*, *43*(2), pp.197-203.
29. Grosse, M., Capa, M. and Bakken, T., 2021. Describing the hidden species diversity of Chaetozone (Annelida, Cirratulidae) in the Norwegian Sea using morphological and molecular diagnostics. *ZooKeys*, *1039*, p.139.Galil, B.S. and Goren, M., 1995. The deep sea Levantine Fauna - New records and rare occurrences. *Senckenbergiana maritima*, *25*(1), pp.41-52.
30. Guerra, A., 2006. Ecology of Sepia officinalis. *Vie et Milieu/Life & Environment*, pp.97-107.
31. Guerra-García, J.M., De Figueroa, J.T., Navarro-Barranco, C., Ros, M., Sánchez-Moyano, J.E. and Moreira, J., 2014. Dietary analysis of the marine Amphipoda (Crustacea: Peracarida) from the Iberian Peninsula. *Journal of Sea Research*, *85*, pp.508-517.

32. Hoffman, L. and Freiwald, A., 2017. A unique and diverse amalgamated mollusk assemblage from the Coral Patch Seamount, eastern Atlantic. *Miscellanea Malacologica*, *7*(4), pp.61-79.
33. Holte, B., 1998. The macrofauna and main functional interactions in the sill basin sediments of the pristine Holandsfjord, northern Norway, with autecological reviews for some key-species. *Sarsia*, *83*(1), pp.55-68.
34. Holthuis, L.B., 1980. The identity of Hapalopoda investigator Filhol, 1885 (Decapoda, Penaeidae) and other shrimps collected by the 1880-1883" Travailleur" and" Talisman" expeditions. *Zoologische Mededelingen*, *55*(15), pp.183-194.
35. Hughes, R.N., 1986. Laboratory observations on the feeding behaviour, reproduction and morphology of Galeodea echinophora (Gastropoda: Cassidae). *Zoological journal of the Linnean Society*, *86*(4), pp.355-365.
36. Ilan, M., Gugel, J., Galil, B.S. and Janussen, D., 2003. Small bathyal sponge species from East Mediterranean revealed by a non-regular soft bottom sampling technique. *Ophelia*, *57*(3), pp.145-160.
37. Kitsos, M.S., 2008. Diet composition of the pandalid shrimp, Plesionika narval (Fabricius, 1787)(Decapoda, Pandalidae) in the Aegean Sea. *Crustaceana*, *81*(1), pp.23-33.
38. Kitsos, M.S., Doulgeraki, S., Tselepides, A. and Koukouras, A., 2005. Diet composition of the bathyal crabs, Chaceon mediterraneus Manning and Holthuis and Geryon longipes A. Milne-Edwards (Decapoda, Geryonidae) collected at different depths in the eastern Mediterranean. *Crustaceana*, *78*(2), pp.171-184.
39. Künitzer, A., Basford, D., Craeymeersch, J.A., Dewarumez, J.M., Dörjes, J., Duineveld, G.C.A., Eleftheriou, A., Heip, C., Herman, P., Kingston, P. and Niermann, U., 1992. The benthic infauna of the North Sea: species distribution and assemblages. *ICES Journal of Marine Science*, *49*(2), pp.127-143.
40. Levin, L.A. and Mendoza, G.F., 2007. Community structure and nutrition of deep methane-seep macrobenthos from the North Pacific (Aleutian) Margin and the Gulf of Mexico (Florida Escarpment). *Marine Ecology*, *28*(1), pp.131-151.
41. Lubinevsky, H., Hyams-Kaphzan, O., Almogi-Labin, A., Silverman, J., Harlavan, Y., Crouvi, O., Herut, B., Kanari, M. and Tom, M., 2017. Deep-sea soft bottom infaunal communities of the Levantine Basin (SE Mediterranean) and their shaping factors. *Marine biology*, *164*(2), pp.1-12.
42. Maynou, F. and Cartes, J.E., 2012. Effects of trawling on fish and invertebrates from deep-sea coral facies of Isidella elongata in the western Mediterranean. *Journal of the Marine Biological Association of the United Kingdom*, *92*(7), pp.1501-1507.
43. Mecho, A., Billett, D.S., Ramírez-Llodra, E., Aguzzi, J. and Tyler, P.A., 2014. First records, rediscovery and compilation of deep-sea echinoderms in the middle and lower continental slope of the Mediterranean Sea.
44. Morton, B., 2016. The biology and functional morphology of the predatory septibranch Cardiomya costellata (Deshayes, 1833)(Bivalvia: Anomalodesmata: Cuspidariidae) from the Açores: survival at the edge. *Journal of the Marine Biological Association of the United Kingdom*, *96*(6), pp.1347-1361.
45. Murina, G.V.V., Pancucci-Papadopoulou, M.A. and Zenetos, A., 1999. The phylum Sipuncula in the eastern Mediterranean: composition, ecology, zoogeography. *Journal of the Marine Biological Association of the United Kingdom*, *79*(5), pp.821-830.

46. Nasto, I., Cardone, F., Mastrototaro, F., Panetta, P., Rosso, A., Sanfilippo, R., Taviani, M. and Tursi, A., 2018. Benthic invertebrates associated with subfossil cold-water coral frames and hardgrounds in the Albanian deep waters (Adriatic Sea). *Turkish Journal of Zoology*, *42*(4), pp.360-371.
47. Navarro-Barranco, C., Tierno-de-Figueroa, J.M., Guerra-García, J.M., Sánchez-Tocino, L. and García-Gómez, J.C., 2013. Feeding habits of amphipods (Crustacea: Malacostraca) from shallow soft bottom communities: Comparison between marine caves and open habitats. *Journal of Sea Research*, *78*, pp.1-7.
48. Negri, M.P. and Corselli, C., 2016. Bathyal Mollusca from the cold-water coral biotope of Santa Maria di Leuca (Apulian margin, southern Italy). *Zootaxa*, *4186*(1), pp.1-97.
49. Öktener, A., Alaş, A. and Türker, D., 2018. First record of Anilocra physodes (Isopoda, Cymothoidae) on the Phycis blennoides (Pisces; Phycidae) with morphological characters and hosts preferences.
50. ÖZTÜRK, B., 2011. Scaphopod species (Mollusca) of the Turkish Levantine and Aegean seas. *Turkish Journal of Zoology*, *35*(2), pp.199-211.
51. Olu-Le Roy, K., Sibuet, M., Fiala-Médioni, A., Gofas, S., Salas, C., Mariotti, A., Foucher, J.P. and Woodside, J., 2004. Cold seep communities in the deep eastern Mediterranean Sea: composition, symbiosis and spatial distribution on mud volcanoes. *Deep Sea Research Part I: Oceanographic Research Papers*, *51*(12), pp.1915-1936.
52. Papaconstantinou, C. and Kapiris, K., 2003. The biology of the giant red shrimp (Aristaeomorpha foliacea) at an unexploited fishing ground in the Greek Ionian Sea. *Fisheries Research*, *62*(1), pp.37-51.
53. Perez Farfante, I.S.A.B.E.L. and Kensley, B., 1997. *Penaeoid and sergestoid shrimps and prawns of the world. Keys and diagnoses for the families and genera*. Editions du Museum national d'Histoire naturelle.
54. Pinho, M.R., Gonçalves, J.M., Martins, H.R. and Menezes, G.M., 2001. Some aspects of the biology of the deep-water crab, Chaceon affinis (Milne-Edwards and Bouvier, 1894) off the Azores. *Fisheries Research*, *51*(2-3), pp.283-295.
55. Por, D. F., 1964. A study of the levantine and pontic harpacticoida (Crustacea, Copepoda). *Zoologische verhandelingen*, *64*(1), pp.1-128.
56. Prato, E. and Biandolino, F., 2005. Amphipod biodiversity of shallow water in the Taranto seas (north-western Ionian Sea). *Journal of the Marine Biological Association of the United Kingdom*, *85*(2), pp.333-338.
57. Raso, J.E.G., García-Muñoz, J.E., Mateo-Ramírez, A., González, N.L., Fernández-Salas, L.M. and Rueda, J.L., 2019. Decapod crustaceans Eucalliacidae in chemoautotrophic bathyal bottoms of the Gulf of Cadiz (Atlantic Ocean), environmental characteristics and associated communities. *Journal of the Marine Biological Association of the United Kingdom*, *99*(2), pp.437-444.
58. Ravara, A., Ramos, D., Teixeira, M.A., Costa, F.O. and Cunha, M.R., 2017. Taxonomy, distribution and ecology of the order Phyllodocida (Annelida, Polychaeta) in deep-sea habitats around the Iberian margin. *Deep Sea Research Part II: Topical Studies in Oceanography*, *137*, pp.207-231.
59. Ritt, B., Desbruyères, D., Caprais, J.C., Gauthier, O., Ruffine, L., Buscail, R., Olu-Le Roy, K. and Sarrazin, J., 2012. Seep communities from two mud volcanoes in the deep eastern

Mediterranean Sea: faunal composition, spatial patterns and environmental control. *Marine Ecology Progress Series*, *466*, pp.93-119.
60. Rodrigues, C.F., Oliver, P.G. and Cunha, M.R., 2008. Thyasiroidea (Mollusca: Bivalvia) from the mud volcanoes of the Gulf of Cadiz (NE Atlantic). *Zootaxa*, *1752*(1), pp.41-56.
61. Salvini-Piawen, L.V. and Ozturk, B., 2006. New records of Caudofoveata (Falcidens gutturosus, Prochaetoderma raduliferum) and of Solenogastres (Eleutheromenia carinata, spec. nov.) from the eastern Mediterranean Sea (Mollusca). *Spixiana*, *29*(3), p.217.
62. Sardá Amills, F., Calafat Frau, A., Flexas, M.D.M., Tselepides, A., Canals Artigas, M., Espino Infantes, M. and Tursi, A., 2004. An introduction to Mediterranean deep-sea biology. *Scientia Marina, 2004, vol. 68, num. suppl 3, p. 7-38*.
63. Southward, E.C., Andersen, A.C. and Hourdez, S., 2011. Lamellibrachia anaximandri n. sp., a new vestimentiferan tubeworm (Annelida) from the Mediterranean, with notes on frenulate tubeworms from the same habitat. *Zoosystema*, *33*(3), pp.245-279.
64. Steiner, G. and Kabat, A.R., 2004. *Catalog of species-group names of Recent and fossil Scaphopoda (Mollusca)*. Paris: Publications Scientifiques du Muséum national d'Histoire naturelle.
65. Tecchio, S., Ramírez-Llodra, E. and Sardà, F., 2011. Biodiversity of deep-sea demersal megafauna in western and central Mediterranean basins. *Scientia Marina*, *75*(2), pp.341-350.
66. TUNÇER, S., ARTÜZ, L., CENGIZ, Ö., ÖNAL, U. and POURSANIDIS, D., First record of the side gill slug Pleurobranchaea meckeli (Blainville, 1825)(Gastropoda: Heterobranchia) from Dardanelles (Çanakkale Strait) and new records from the Sea of Marmara, Turkey.
67. Vacelet, J. 1987 Eponges. p. 137-148. In Fischer, W., M. L. Bauchot and M. Schneider. 1987. Fiches FAO d' identification des espèces pour les besoins de la pêche. (Revision 1). Méditerranée et mer Noire. Zone de pêche 37. Volume I. Végëtaux et Invertébrés. Publication préparée par la FAO, résultant d'un accord entre la FAO et la Commission des Communautés européennes (Project GCP/INT/422/EEC) financëe conjointement par ces deux organisations. Rome, FAO, Vol.1.
68. Walker, A.J.M. and E.I.S. Rees 1980 Benthic ecology of Dublin Bay in relation to sludge dumping. Irish Fisheries Investigations. Series B. 22:1-59.

Annex 6

Delineation of unknown biological assemblage areas OR why biological assemblage in a specific geomorphic domain cannot be used to characterize biology of the entire geomorphic domain.

In the project's steering committee meeting held on Thursday November 17th, the authors were asked by one of the members why an entire geomorphic domain was not biologically characterized based on the biological assemblages that were found in it. Specifically, the intention was to characterize the "unknown" area in the "main deep-sea fan" domain as "bathyal plain assemblage" (Figure A11).

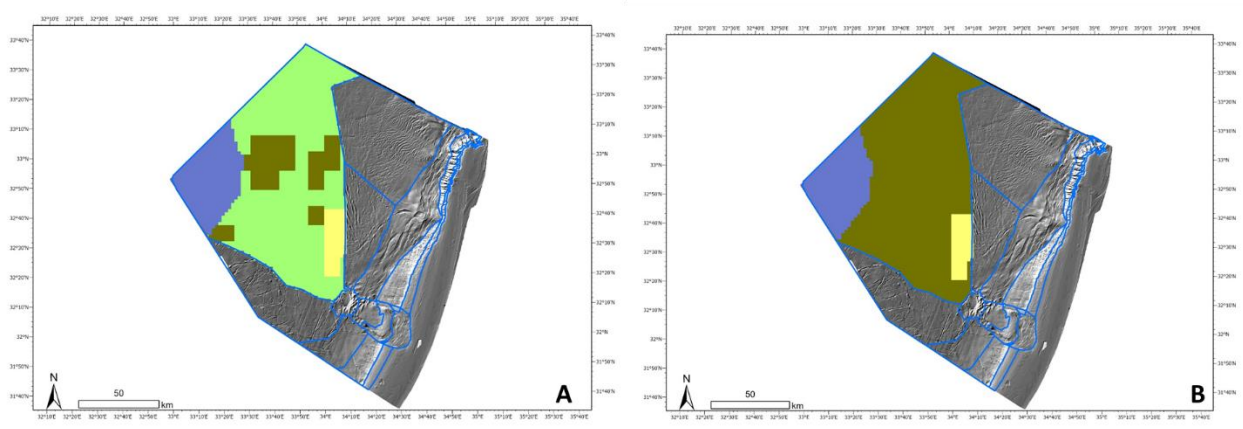

Figure A11. Merged ecological units in the Main deep-sea fan domain as suggested by the authors (A), and by the steering committee member (B), where the "unknown main deep-sea fan ecological unit is characterized as "bathyal plain" biological assemblage and the two are merged to form a single ecological unit- "Bathyal plain-main deep-sea fan"

The delineation of the units was performed by overlaying data layers of all hierarchical classification levels. The lowest (most detailed) level was of the biological assemblages in the area. Areas where biological data was available, were characterized as distinct ecological units from their surrounding that was often of the same class in higher hierarchical levels. For example, in the third hierarchical level of geomorphic domains, the "Main deep sea fan" (Figure A12), two distinct biological assemblages were found[1]: "Soft-bottom sponge ground assemblage" and " Bathyal plain assemblage" (Figure A13).

[1] The fourth hierarchical level of sediment types was not informative enough for distinction between areas within this domain, but it was used in the GDM to support decisions regarding delineation of the ecological units

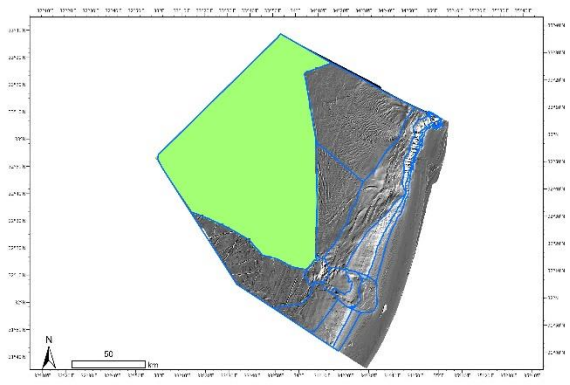

Figure A12. The main deep-sea fan geomorphic domain.

Figure A13. Biological assemblages overlapping the Main deep-sea fan geomorphic domain. Two assemblages were identified: Soft-bottom sponge ground (orange) and Bathyal plain (light purple).

Accordingly, delineation of the ecological units produced three units for the “Main deep Sea fan” domain (Figure A14A):

1- Ecological unit where biological assemblage was of type “soft-bottom sponge ground”
2- Ecological unit where biological assemblage was of type “Bathyal plain”
3- Ecological unit where the biological assemblage was unknown

Later, we further divided the “unknown area” to include foraminiferous assemblage in the western corner. This was supported by the GDM results (Figure A14B, Figure A15).

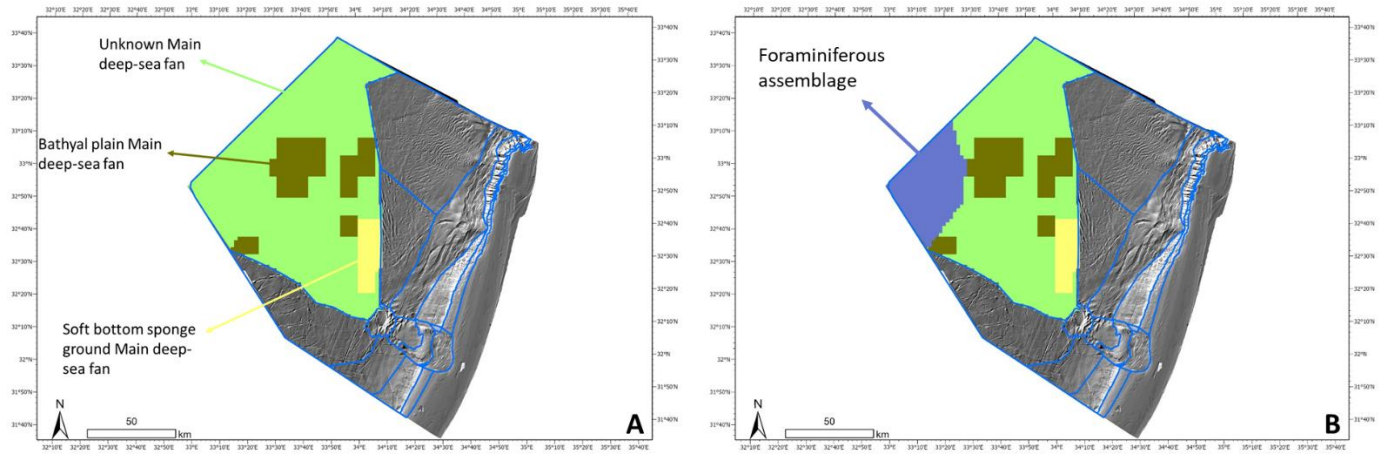

Figure A14. A. Ecological units in the Main deep-sea fan domain based on biological assemblages identified following cluster analysis of biological data from the Israeli EEZ area. **B.** Foraminiferous assemblage that was added as distinct ecological unit within the Main deep-sea fan domain following Hyams-Kaphzan et al. (2018) and based on the GDM results.

The argument for the suggestion to merge these units was derived from the notion that the bathyal plain assemblage seems to be similar to its surrounding in all higher hierarchical levels and according to the GDM. However, we suggest that keeping these units separate is important because of the following arguments:

1- In the "Main deep-sea fan" geomorphic domain there are at least three distinct biological assemblages: Soft bottom sponge ground assemblage", " Bathyal plain assemblage", and "Foraminiferous assemblage". The "unknown area" could belong to any of these (See Figure A15C). Thus, the variables used in the GDM cannot fully predict the biological diversity in the area.
2- Extrapolating biological assemblage to an area of ~7000 km^2 that was almost never explored can lead to seriously biased distribution of the ecological units. It is critical to be clear in all further analyses that this area is truly unknown at this stage.
3- The GDM results suggest that the north-western corner of the EEZ differs from it surrounding (characterized by bathymetric, abiotic and sediment features. See Figure A15). This further demonstrate how the "unknown area" may differ from the "bathyal plain assemblage" area.

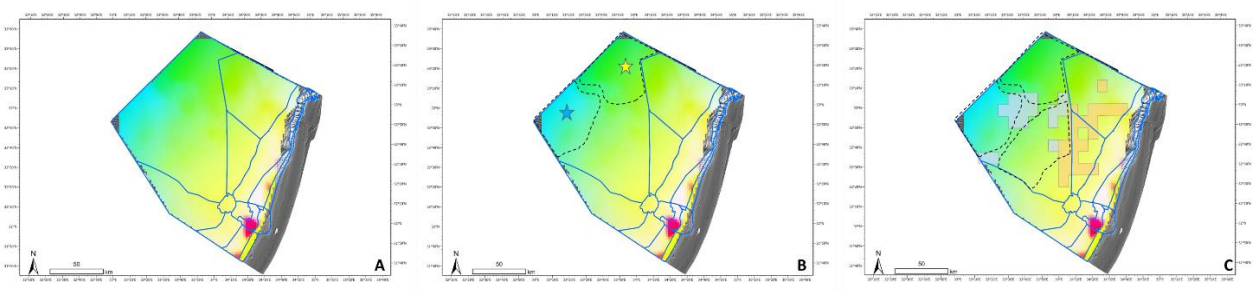

Figure A15. The GDM results (A), suggest that the north-western corner of the EEZ (B- marked by yellow star) differs from it surrounding (characterized by bathymetric, abiotic and sediment features). However, there are no biological data from this area to support splitting of the “unknown area” as was done for the Foraminiferous area (B- marked by blue star) into two distinct ecological units. C. dashed lines mark areas that the GDM identified as distinct. And further demonstrate how the “unknown area” or parts of it, may differ from the “bathyal plain assemblage” area.